BMC Biology

RESEARCH

Open Access

The circular RNA *circbabo(5,6,7,8S)* regulates lipid metabolism and neuronal integrity via TGF-β/ROS/JNK/SREBP signaling axis in *Drosophila*

Jie Sheng[1], Xuemei Zhang[1], Weihong Liang[2], Junfang Lyu[1], Bei Zhang[2], Jie Min[2], Austin Xu[2], Xingyu Xu[1], Jennifer W. Li[3], Jian-Liang Li[4], Rui Zhou[2*] and Wei Liu[1,2*]

Abstract

Background Lipid droplets (LDs) are dynamic cytoplasmic lipid-storing organelles that play a pivotal role in maintaining cellular energy balance, lipid homeostasis, and metabolic signaling. Dysregulation of lipid metabolism, particularly excessive lipogenesis, contributes to the abnormal accumulation of LDs in the nervous system, which is associated with several neurodegenerative diseases. Circular RNAs (circRNAs) are a new class of non-coding and regulatory RNAs that are widely expressed in eukaryotes. However, only a subset has been functionally characterized. Here, we identified and functionally characterized a new circular RNA *circbabo(5,6,7,8S)* that regulates lipogenesis and neuronal integrity in *Drosophila melanogaster*.

Results *circbabo(5,6,7,8S)* is derived from the *babo* locus which encodes the type I receptor for transforming growth factor β (TGF-β). Depletion of *circbabo(5,6,7,8S)* in flies causes elevated lipid droplet accumulation, progressive photoreceptor cell loss and shortened lifespan, phenotypes that are rescued by restoring *circbabo(5,6,7,8S)* expression. In addition, RNA-seq and epistasis analyses reveal that these abnormalities are caused by aberrant activation of the SREBP signaling pathway. Furthermore, *circbabo(5,6,7,8S)*-depleted tissues display enhanced activation of the TGF-β signaling pathway and compromised mitochondrial function, resulting in upregulation of reactive oxygen species (ROS). Moreover, we provide evidence that *circbabo(5,6,7,8S)* encodes the protein circbabo(5,6,7,8S)-p, which inhibits TGF-β signaling by interfering with the assembly of babo/put receptor heterodimer complex. Lastly, we show that dysregulation of the ROS/JNK/SREBP signaling cascade is responsible for the LD accumulation, neurodegeneration, and shortened lifespan phenotypes elicited by *circbabo(5,6,7,8S)* depletion.

Conclusions Our study demonstrates the physiological role of the protein-coding circRNA *circbabo(5,6,7,8S)* in regulating lipid metabolism and neuronal integrity.

Keywords *circbabo(5,6,7,8S)*, Lipid metabolism, Neuronal integrity, TGF-β, SREBP, *Drosophila*

*Correspondence:
Rui Zhou
rzhou13@jhmi.edu
Wei Liu
wliu@xzhmu.edu.cn
Full list of author information is available at the end of the article

Background

Lipid metabolism and energy homeostasis are vital for the health of living organisms [1]. Triacylglycerols (TG) and cholesterol esters (CEs) are the primary storage lipids in lipid droplets (LDs) of eukaryotic cells [2]. LDs are dynamic cytoplasmic organelles that play a pivotal role in maintaining cellular energy balance, lipid homeostasis, and signaling [2–5]. In mammals, LDs are abundant in adipose and liver tissues. In insects such as the fruit fly *Drosophila melanogaster*, fat body is the primary fat storage tissue, which contains numerous, variably sized LDs. The nervous system, including neurons and glial cells, also contains high concentrations of lipids [6, 7]. It has been reported that abnormal accumulation of LDs in the nervous system is associated with several neurodegenerative diseases [8–11]. For example, abnormalities in the lipolysis pathway can lead to the accumulation of LDs in cells [12, 13]. In the fruit fly model of Parkinson's disease, the lipid droplet membrane protein dPlin1/2 inhibits lipolysis, leading to the accumulation of LDs and the aggregation of pathogenic α-Syn proteins in neurons [14]. In addition, lipophagy is a selective form of autophagy that degrades LDs within the lysosomes [15]. Inhibiting lipophagy can result in LD accumulation in the nervous system of model organisms such as fruit flies and mice, leading to neurodegeneration [16–19].

Excessive lipogenesis can also result in abnormal accumulation of LDs in the nervous system [20]. Sterol regulatory element binding protein (SREBP) is a key transcription factor for LD biogenesis. The proteolytically cleaved and activated form of SREBP enters the nucleus and promotes the expression of lipogenic genes, including *ATP citrate lyase* (*ATPCL*), *acetyl-CoA carboxylase* (*ACACA*), and *fatty acid synthase* (*FASN*) [21]. During the TCA cycle, citrate is formed and exported from the mitochondria. ATPCL and ACACA catalyze the formation of acetyl-CoA and malonyl-CoA from citrate. Malonyl-CoA then undergoes a series of decarboxyl-CoA Claisen condensations with FASN to produce palmitic acid (16:0), which is an essential precursor for other fatty acids [22]. However, an excess of fatty acids can be harmful to cells and lead to lipotoxicity. Therefore, most cells store fatty acids as TG in LDs [23]. The SREBP pathway is highly regulated [24]. For example, high glucose and insulin levels activate SREBP, promoting lipogenesis via PI3K-AKT and mTOR pathways in well-fed conditions [25, 26]. In addition, mitochondrial dysfunction leads to LD accumulation in glial cells via the ROS/JNK/SREBP signaling cascade, which accompanies neurodegeneration in *Drosophila* [27].

An increasing number of non-coding RNAs (ncRNAs) have been implicated in a wide variety of biological processes [28, 29], including the regulation of lipid metabolism through the action of SREBP. For example, loss of *miR-210* causes aberrant activation of the SREBP signaling pathway, leading to LD accumulation and retinal degeneration in *Drosophila* [30]. In addition, long non-coding RNA (lncRNA) *H19* alters cellular lipid metabolism by binding to polypyrimidine tract-binding protein 1 (PTBP1), leading enhanced transcriptional activation by SREBP-1 in mammalian hepatocytes [31]. In recent years, a new class of non-coding and regulatory RNAs, known as circular RNAs (circRNAs), have been found widely expressed in eukaryotes. circRNAs are involved in myriad biological processes such as innate immunity, neurodevelopment, gene expression, and lipid metabolism [32–37]. In particular, *circPRKAA1* triggers lipid accumulation through the Ku80/Ku70/SREBP-1 signaling cascade in colon cancer cells [38]. However, examples of circRNAs regulating the SREBP pathway in the nervous system are still limited.

Previously, we identified a number of circRNAs in *Drosophila* that regulate innate immunity and neurodevelopment [32, 33, 37]. Among our circRNA collection is *circbabo(5,6,7,8S)*, which is derived from the *babo* locus. In this study, we report that depletion of *circbabo(5,6,7,8S)* in flies causes elevated LD accumulation, progressive photoreceptor cell loss and shortened lifespan. We show that these abnormalities are caused by aberrant activation of the SREBP signaling pathway. In addition, *circbabo(5,6,7,8S)*-depleted tissues display enhanced TGF-β signaling, which inhibits mitochondrial function, leading to a reduction in ATP levels and an increase in ROS. Mechanistically, we present evidence that *circbabo(5,6,7,8S)* regulates the TGF-β signaling pathway through a functional protein encoded by this circRNA. Lastly, we show that the ROS/JNK/SREBP signaling cascade is responsible for the metabolism and neurodegeneration phenotypes of *circbabo(5,6,7,8S)*-depleted flies. Taken together, our study reveals a crucial function of *circbabo(5,6,7,8S)* in regulating the TGF-β/ROS/JNK/SREBP axis to impact lipid metabolism and neuronal integrity in *Drosophila*.

Results

Validation of circRNA*circbabo(5,6,7,8S)* in *Drosophila*

Among the circRNA candidates identified in our previous study [32] is *circbabo(5,6,7,8S)*. *circbabo(5,6,7,8S)* is derived from the *babo* gene, which encodes the type I receptor babo of TGF-β signaling (Fig. 1A). *circbabo(5,6,7,8S)* is a product of backsplicing reaction involving the splice site upstream of exon 5 and a cryptic 5' splice site within the annotated exon 8, joining the 3' end of exon 8S with the 5' end of exon 5 (Fig. 1A, B). A pair of divergent primers derived from exons 5 and 8S were able to amplify products from cDNA templates,

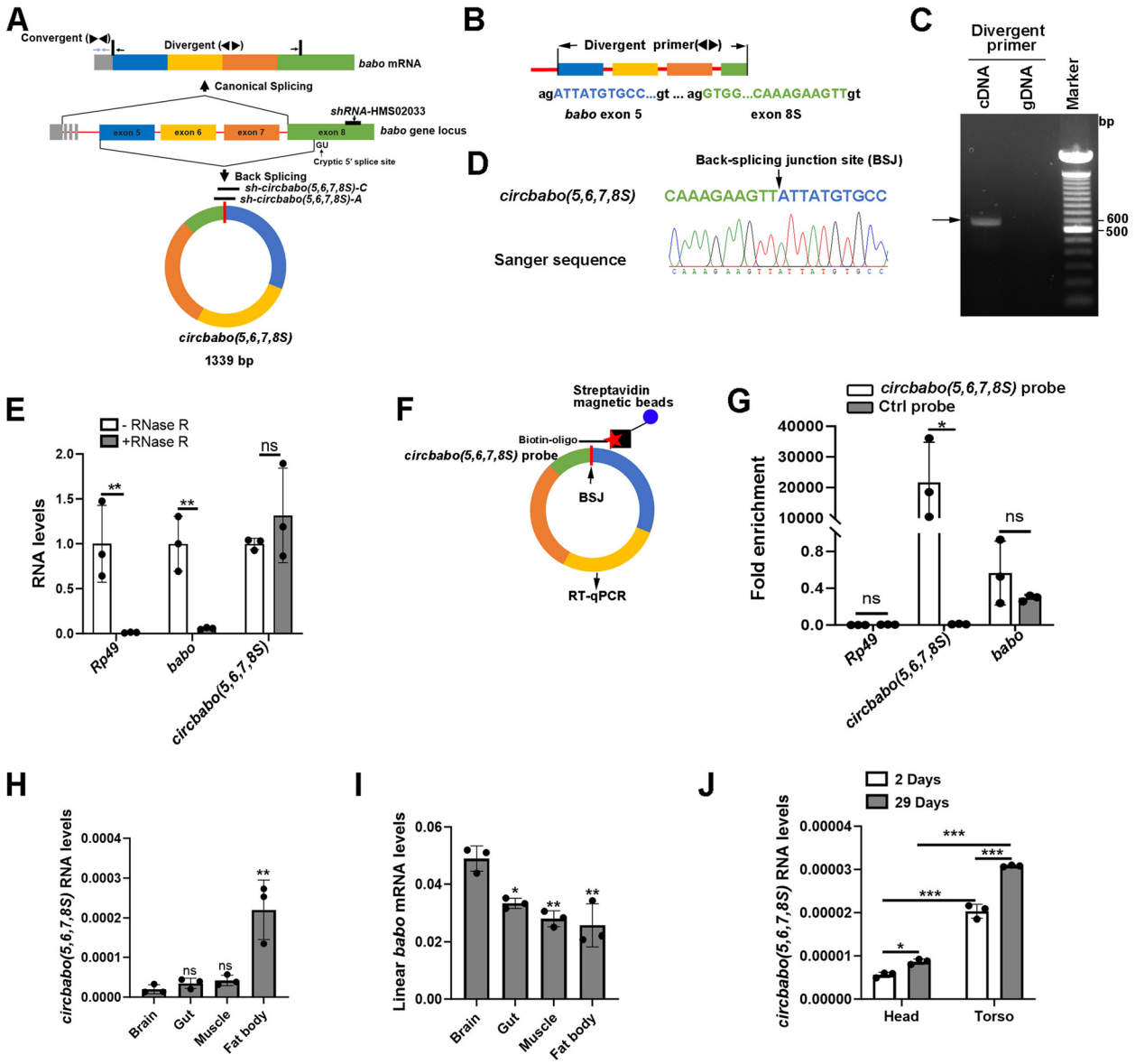

Fig. 1 Validation of circRNA *circbabo(5,6,7,8S)*. **A** A diagram showing *circbabo(5,6,7,8S)* and the linear *babo* mRNA derived from the *babo* locus as well as mapping of various shRNA reagents and various oligos. A cryptic 5′ splice site within exon 8 is utilized to generate *circbabo(5,6,7,8S)*. Thick and thin bars represent exons and introns, respectively. **B** Divergent primers are shown on the top, which are derived from exons 5 (blue) and 8S (green). **C** Divergent primers amplify circRNA-derived products from cDNA template. No products were amplified from genomic DNA (gDNA) template. **D** Sanger sequencing confirms the head-to-tail back splice junction in *circbabo(5,6,7,8S)*. **E** *circbabo(5,6,7,8S)* is resistant to RNase R treatment. After RNase R treatment and before reverse transcription, a small amount of mouse brain total RNA was added as "spike-in" controls. Levels of the *circbabo(5,6,7,8S)* and the linear mRNAs were quantified by qPCR. All the indicated RNAs were normalized to the mouse *gapdh* mRNA (Student's *t* test, $n = 3$, ** $p < 0.01$; ns, non-significant). **F** A diagram showing the biotinylated probe complementary to the back-spliced exon junction (BSJ) of *circbabo(5,6,7,8S)*. Streptavidin conjugated magnetic beads were used to purify the biotin-probe/circRNA complexes. **G** A biotinylated *circbabo(5,6,7,8S)* probe pulled down *circbabo(5,6,7,8S)*. A control pull-down was performed using a biotinylated DNA probe that is sense to the back-spliced exon junction of *circbabo(5,6,7,8S)*. After reverse transcription of the purified RNA, qPCR was performed to quantify the RNA levels (Student's *t* test, $n = 3$, * $p < 0.05$; ns, non-significant). **H, I** Total RNA was prepared from various dissected tissues of third-instar larvae, and levels of *circbabo(5,6,7,8S)* (**H**) and linear *babo* mRNA (**I**) were measured (one-way ANOVA with Turkey post hoc test, $n = 3$, * $p < 0.05$; ** $p < 0.01$; ns, non-significant). **J** Total RNA was prepared from fly heads and torso samples of young (2-day) and old (29-day) animals, and levels of the *circbabo(5,6,7,8S)* were measured (one-way ANOVA with Turkey post hoc test, $n = 3$, * $p < 0.05$; *** $p < 0.001$)

but not from genomic DNA (gDNA) (Fig. 1B, C). In addition, Sanger sequencing confirmed the unique back-spliced exon junction (Fig. 1D). Furthermore, we performed RNase R treatment, which revealed that *circbabo(5,6,7,8S)* is resistant, whereas the linear mRNAs (*Rp49* and *babo*) are susceptible to RNase R-mediated degradation (Fig. 1E). Moreover, to further validate *circbabo(5,6,7,8S)*, a biotinylated oligo probe complementary to the unique back-spliced exon junction of *circbabo(5,6,7,8S)* was employed to purify the endogenous *circbabo(5,6,7,8S)* from *Drosophila S*chneider *L*ine *2* (SL2) cell lysate (Fig. 1F). RT-qPCR analysis revealed that *circbabo(5,6,7,8S)* was specifically pulled down by this antisense probe, but not by a control sense probe (Fig. 1G). Lastly, Sanger sequencing uncovered that *circbabo(5,6,7,8S)* is 1339 nt in length. Taken together, results from RT-PCR with divergent primers, Sanger sequencing, RNase R resistance analyses, and circRNA pull-down assay confirmed that *circbabo(5,6,7,8S)* is a circRNA containing four exonic segments from the *babo* locus (Fig. 1A; Additional file 1: Table S1).

Next, we analyzed the expression pattern of *circbabo(5,6,7,8S)* in different tissues. Total RNA was isolated from various larval organs/tissues, including the gut, brain, fat body, and muscle, followed by RT-qPCR. While *circbabo(5,6,7,8S)* and its linear sibling *babo* are present in all these tissues, they exhibit distinct expression patterns (Fig. 1H, I). Notably, *circbabo(5,6,7,8S)* is highly expressed in the fat body, with levels nearly 7 times higher than in the brain (Fig. 1H). In contrast, levels of the linear *babo* transcript are higher in the brain than in the fat body (Fig. 1I). We also detected fourfold higher levels of *circbabo(5,6,7,8S)* in the adult torso than in the fly head (Fig. 1J). In addition, our analysis reveals that levels of *circbabo(5,6,7,8S)* display a significant increase with age (Fig. 1J). Given that circRNAs are typically more stable than their linear counterparts, the observed increase in circRNA levels with age may be attributed, at least in part, to the differences in stability between circular and linear RNAs.

circbabo(5,6,7,8S) depletion leads to lipid accumulation in *Drosophila* fat body cells

The *Drosophila* fat body stores excess energy in the form of triglycerides, similar to the white adipose tissue in mammals. The high expression level of *circbabo(5,6,7,8S)* in the larval fat body prompted us to investigate whether it is involved in lipid metabolism. Two independent transgenic small hairpin RNA (shRNA) lines were generated that target the back-spliced exon junction site. *shcircbabo(5,6,7,8S)* animals were crossed with fat body driver lines, *cg-Gal4*, female larval progenies were collected, and RT-qPCR was performed to measure levels of various RNAs. As expected, *circbabo(5,6,7,8S)* was efficiently knocked down in *cg > shcircbabo(5,6,7,8S)-A* animals while levels of the linear *babo* transcript remained unchanged (Fig. 2A). The loss of *circbabo(5,6,7,8S)* resulted in LD accumulation in the fat body, as revealed by the enlarged LD size (Fig. 2B, C, F). In addition, we generated and analyzed a second *shcircbabo(5,6,7,8S)-C* transgene and similar phenotypes were observed, thereby ruling out off-target effects (Additional file 2: Fig. S1A-C). Biochemical assays also confirmed an increase in triglyceride levels in *cg > shcircbabo(5,6,7,8S)-A* and *-C* fat body, compared with controls (Fig. 2G; Additional file 2: Fig.S1D). Since these two lines exhibited almost identical phenotypes, we selected the *shcircbabo(5,6,7,8S)-A* transgenic line for further analysis. We also use a second fat body driver, *ppl-Gal4* to validate the results from *cg-Gal4*. Depletion of *circbabo(5,6,7,8S)* under control of *ppl-Gal4* induces LD accumulation and increased triglyceride levels in fat body (Additional file 2: Fig. S1F-J),

(See figure on next page.)

Fig. 2 *circbabo(5,6,7,8S)* depletion impacts lipid metabolism. **A** The *UAS-shcircbabo(5,6,7,8S)-A* or the control *UAS-shGFP* transgenic flies were crossed to *cg > Gal4* driver flies. Total RNA was extracted from the fat body samples of the indicated genotypes, and levels of *circbabo(5,6,7,8S)* and linear *babo* mRNA were measured (Student's *t* test, $n = 3$, ** $p < 0.01$; ns, non-significant). **B**–**D** Confocal images of the wandering 3rd *instar* larval fat body from animals expressing control *shGFP* (**B**), *shcircbabo(5,6,7,8S)-A* (**C**), or *shbabo* (**D**) driven by *cg-Gal4*. Nile red and DAPI staining, respectively, labels neutral lipids and nuclei. Scale bar, 50 µm. **E** The *UAS-shbabo* or the control *UAS-shGFP* transgenic flies were crossed to *cg > Gal4* driver flies. Total RNA was extracted from the fat body samples of the indicated genotypes, and levels of *circbabo(5,6,7,8S)* and linear *babo* mRNA were measured (Student's *t* test, $n = 3$, * $p < 0.05$; ns, non-significant). **F** The size of LDs in fat bodies (**B**, **C**, **D**) was quantified (Student's *t* test, $n = 5$, *** $p < 0.001$). **G,H** Samples were collected from the fat bodies of third-instar larvae carrying various UAS transgenes driven by *cg-Gal4*, and TG levels were measured and normalized to protein levels (Student's *t* test, $n = 3$–4, * $p < 0.05$). **I**–**P** Flies carrying the fat body-specific *cg-Gal4* driver were crossed to various combinations of the *UAS-shcircbabo(5,6,7,8S)-A*, control *UAS-shGFP*, empty vector or the *UAS-circbabo(5,6,7,8S)* transgene. Total RNA was prepared from the fat bodies of third-*instar* larvae, and levels of *circbabo(5,6,7,8S)* (**I**) and linear *babo* mRNA (**J**) were measured (one-way ANOVA with Turkey post hoc test, $n = 3$, * $p < 0.05$; ** $p < 0.01$; *** $p < 0.001$; ns, non-significant). Fat bodies from 3rd *instar* larvae of the indicated genotypes were collected (**K**–**N**). Nile red and DAPI staining, respectively, label neutral lipids and nuclei. Scale bar, 50 µm. The size of LDs in fat bodies (from **K**, **L**, **M, N**) was quantified (**O**) (one-way ANOVA with Turkey post hoc test, $n = 3$, *** $p < 0.001$; ns, non-significant). In addition, TG levels in fat bodies of a similar set of samples as in **K**, **L**, **M,** and **N** were measured and normalized to protein levels (**P**) (one-way ANOVA with Turkey post hoc test, $n = 3$, * $p < 0.05$; ** $p < 0.01$; ns, non-significant)

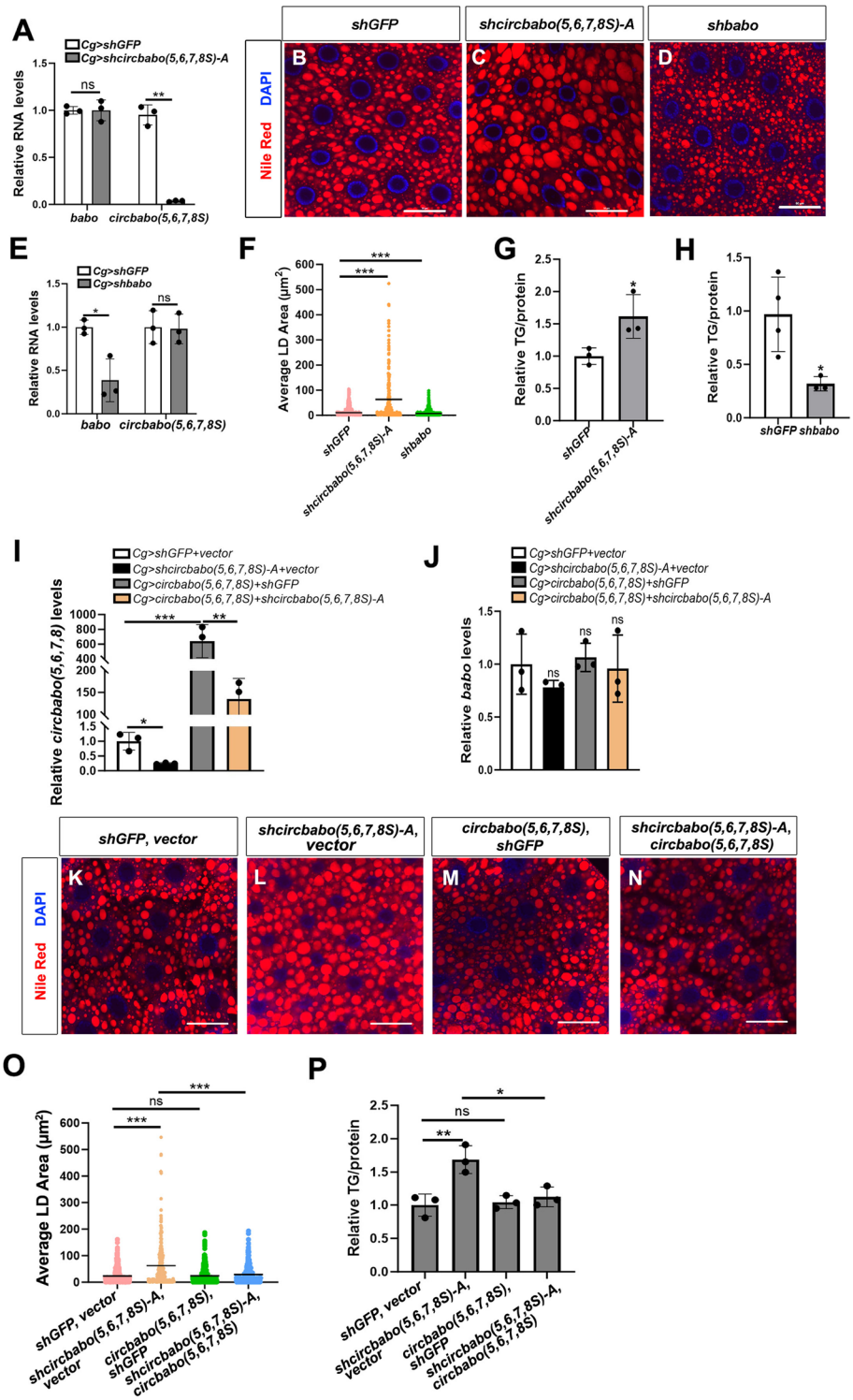

Fig. 2 (See legend on previous page.)

which are consistent with the phenotypes observed in *cg>shcircbabo(5,6,7,8S)* animals. Next, we examined the impact of depleting the linear *babo* transcript in the fat body using a transgenic shRNA line. The linear *babo* transcript was effectively depleted, while levels of *circbabo(5,6,7,8S)* remained unaltered in *cg>shbabo*

animals (Fig. 2E). Notably, knocking down *babo* resulted in decreased LD size and TG storage in the fat body (Fig. 2D–F, H), consistent with previous findings that flies depleted of *babo* display reduced lipid storage in the fat body [39].

To further confirm the role of *circbabo(5,6,7,8S)* in lipid metabolism, we generated flies carrying the *circbabo(5,6,7,8S)* transgene under the control of *u*pstream *a*ctivating *s*equence (UAS). We first crossed various combinations of *shcircbabo(5,6,7,8S)*, *shGFP* (control), *circbabo(5,6,7,8S)*, and empty vector (control) transgenes with *cg-Gal4* flies. The fat body cells from female 3rd *instar* larvae were collected, total RNA was extracted, and RT-qPCR was employed to measure levels of various RNAs. As expected, *cg > shcircbabo(5,6,7,8S)-A* animals showed efficient knockdown of *circbabo(5,6,7,8S)* while levels of the linear *babo* remained unchanged (Fig. 2I, J). Importantly, restoring *circbabo(5,6,7,8S)* expression in *circbabo(5,6,7,8S)*-depleted cells rescued the LD accumulation phenotype, indicating that the phenotypes elicited by *circbabo(5,6,7,8S)*-depletion were on-target effects (Fig. 2K–P). Taken together, these results demonstrate the essential role of *circbabo(5,6,7,8S)* in maintaining lipid homeostasis in the larval fat body.

circbabo(5,6,7,8S) impacts neuronal integrity and animal survival

Imbalances in lipid metabolism in neuronal systems are strongly associated with the initiation and progression of neurodegenerative diseases [40]. Given that *circbabo(5,6,7,8S)* functions in adipose tissue to regulate lipid metabolism, we further explored the underlying role of *circbabo(5,6,7,8S)* in the nervous system. The neurons in the eyes of adult *Drosophila* are highly organized, allowing for easy assessment of any disruption in neural function caused by genetic alterations in vivo. Therefore, we crossed various combinations of *shcircbabo(5,6,7,8S)-A*, *shGFP* (control), *circbabo(5,6,7,8S)*, and empty vector (control) transgenes with flies carrying the eye-specific *GMR-Gal4* driver. The heads of young (3 days) and old (30 days) adult flies were collected for TEM analysis (Fig. 3A–H). Rhabdomere loss was observed in a few ommatidia of 3-day-old *GMR > shcircbabo(5,6,7,8S)-A* fly eyes, but not in control flies (Fig. 3A, B, G). Moreover, moderate rhabdomere loss was detected in the lamina cartridges in the eyes of 30-day-old *GMR > shcircbabo(5,6,7,8S)-A* flies, whereas the control samples are normal (Fig. 3D, E, H). Notably, we detected lipid droplet accumulation in the photoreceptor cells of 3-day-old *GMR > shcircbabo(5,6,7,8S)-A* flies, but not in control animals (Fig. 3A'–B', I, indicated by arrows), suggesting that *circbabo(5,6,7,8S)* regulates lipid metabolism in retinas as well. Interestingly, no lipid droplet accumulation was detected in aged *GMR > shcircbabo(5,6,7,8S)-A* flies (Fig. 3D'–E', I), which is consistent with the notion that LD accumulation represents an early, transient indicator/promoter of neurodegenerative disease [27]. Besides TEM analysis, we also visualized LDs using Nile red, and detected LD accumulation in the ommatidia of 3-day-old *GMR > shcircbabo(5,6,7,8S)* flies (Additional file 3: Fig. S2B, S2E-F). Notably, the eye degeneration and LD accumulation phenotypes in *circbabo(5,6,7,8S)*-depleted flies were rescued upon restoring *circbabo(5,6,7,8S)* expression (Fig. 3C, C', F, G–I, Additional file 3: Fig. S2A-C). Interestingly, in the 3-day-old *GMR > shcircbabo(5,6,7,8S)-A* flies we found that majority of LDs were localized in neurons (Additional file 3: Fig. S2E, S2G), whereas only a small proportion of LDs were detected in the glia (Additional file 3: Fig. S2F, S2G). It has been reported that *babo* is expressed in both glial cells and neurons [41]. Therefore, it is highly likely that circbabo(5,6,7,8S) is expressed in both cell types as well. To analyze the role of *circbabo(5,6,7,8S)* in glia, we knocked down *circbabo(5,6,7,8S)* in the glia using the *repo-Gal4* driver and found that the glial *circbabo(5,6,7,8S)* depletion led to photoreceptor cell loss (Additional file 3: Fig. S2H-K). In contrast, we did not detect retinal LD accumulation (Additional file 3: Fig. S2I). These data suggested that the expression of *circbabo(5,6,7,8S)* in glia facilitates to maintain neuronal integrity. In addition, we knocked down *circbabo(5,6,7,8S)* using the pan-neuronal *elav-Gal4* and detected LD accumulation in the photoreceptor cells of young flies, but not in control animals (Additional file 3: Fig. S2L-M, S2T). Moreover, retinal degeneration was detected in the lamina cartridges in the eyes of old *elav > shcircbabo(5,6,7,8S)* flies, whereas the control samples are normal (Additional file 3: Fig. S2O-P, S2R-S). Lastly, the eye degeneration and LD accumulation phenotypes in *elav > shcircbabo(5,6,7,8S)* flies were rescued upon restoring *circbabo(5,6,7,8S)* expression (Additional file 3: Fig. S2N, S2Q, S2R-T). Thus, although *circbabo(5,6,7,8S)* is not as highly expressed in the brain compared to fat body cells (Fig. 1H), our data demonstrate that it still plays a crucial role in maintaining neuronal integrity and lipid homeostasis.

Neuronal dysfunction is often associated with shortened lifespan in *Drosophila*. Thus, we knocked down *circbabo(5,6,7,8S)* in neurons by crossing the *shcircbabo(5,6,7,8S)-A* transgene with a second pan-neuronal driver *nSyb-Gal4*. Female progenies were collected for the lifespan analysis. Compared with the control animals (*nSyb > shGFP*), *nSyb > shcircbabo(5,6,7,8S)-A* animals displayed shortened lifespan. Importantly, this phenotype can be rescued by restoring *circbabo(5,6,7,8S)* levels in *nSyb > shcircbabo(5,6,7,8S)-A* animals (Fig. 3J).

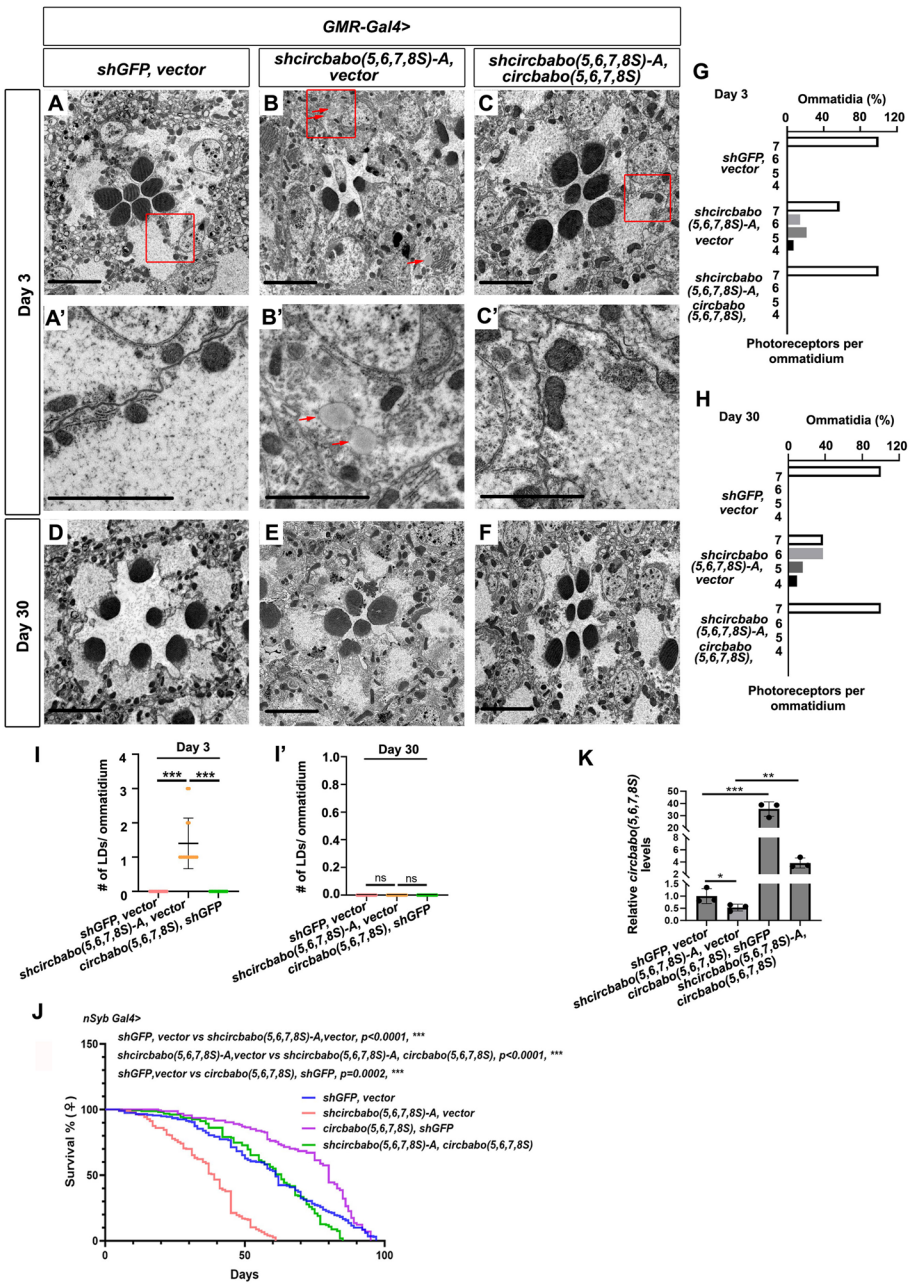

Fig. 3 *circbabo(5,6,7,8S)* depletion causes photoreceptor degeneration. **A–F** Flies carrying the eye-specific *GMR-Gal4* driver were crossed to *UAS-shcircbabo(5,6,7,8S)-A* or control *UAS-shGFP* flies together with the empty vector or the *UAS-circbabo(5,6,7,8S)* transgene. The eyes of 3-day (**A–C**) or 30-day old (**D–F**) flies with the indicated genotypes were analyzed by TEM. Ommatidia were slightly affected at day 3 when *circbabo(5,6,7,8S)* was knocked down but showed moderate degeneration at day 30. The defects were rescued by introducing the *UAS-circbabo(5,6,7,8S)* transgene. The red arrows indicate the lipid droplet structure that was detected in the 3-day-old *GMR > shcircbabo(5,6,7,8S)-A* flies. Scale bar, 5 μm. **A′–C′** Enlarged views of the boxed regions of **A–C**. Scale bar, 2.5 μm. **G, H** Quantification of the number of intact photoreceptors in each ommatidium from flies with the indicated genotypes of **A–F**. Different number of (**A** = 13, **B** = 14, **C** = 13, **D** = 19, **E** = 32, **F** = 15) ommatidia were counted. **I, I′** Quantification of the number of LDs in each ommatidium from flies with the indicated genotypes. **J** Flies carrying the pan neuronal-specific *nSyb-Gal4* driver were crossed to *UAS-shcircbabo(5,6,7,8S)-A* or control *UAS-shGFP* flies together with the empty vector or *UAS-circbabo(5,6,7,8S)* overexpression transgenes. The lifespan of flies of indicated genotypes is shown (*n* represents number of groups for each genotype, 16–20 flies for each group. *shGFP, vector* = 10; *shcircbabo(5,6,7,8S)-A, vector* = 10; *circbabo(5,6,7,8S), shGFP* = 8; *shcircbabo(5,6,7,8S), circbabo(5,6,7,8S)* = 8). **K** Levels of *circbabo(5,6,7,8S)* in flies of the indicated genotypes were measured (one-way ANOVA with Turkey post hoc test, $n = 3$, * $p < 0.05$; ** $p < 0.01$; *** $p < 0.001$)

Furthermore, RT-qPCR confirmed the relative expression levels of *circbabo(5,6,7,8S)* in neurons with indicated genotypes (Fig. 3K). We conclude that neuronal *circbabo(5,6,7,8S)* is essential for maintaining neuronal health and animal survival.

Activation of SREBP signaling in *circbabo(5,6,7,8S)*-depleted flies contributes to LD accumulation

To identify potential effector genes that act downstream of *circbabo(5,6,7,8S)* to impact lipid metabolism, we performed RNA-seq to compare the RNA expression profile in the fat body of *cg > shcircbabo(5,6,7,8S)-A* larvae with that of *cg > shGFP* control animals. In total, 1405 transcripts displayed significant changes in expression upon *circbabo(5,6,7,8S)* depletion, including 449 upregulated transcripts and 956 downregulated transcripts (Fig. 4A; Additional file 4: Table S2). Functional enrichment analysis of the upregulated genes revealed several important gene ontology (GO) categories. Notably, lipid homeostasis was among the top ten enriched functional terms (Fig. 4B). Genes that show increased expression in lipid homeostasis include SREBP, an important regulator of lipogenesis, along with known SREBP targets such as ATPCL and Fasn1 (Fig. 4A), which are responsible for de novo fatty acid synthesis [42, 43]. We selected 8 genes relevant to lipid metabolism and conducted RT-qPCR to assess their expression levels in *cg > shcircbabo(5,6,7,8S)-A* fat body cells. Notably, we detected higher levels of *SREBP*, *ATPCL*, and *Fasn1* transcripts in *circbabo(5,6,7,8S)*-depleted tissues than in control samples (Fig. 4C), suggesting a potential role of SREBP signaling in the LD accumulation phenotype observed in the *circbabo(5,6,7,8S)*-depleted flies. Next, we performed immunoblot using lysates from *cg > shcircbabo(5,6,7,8S)-A* and the control *cg > shGFP* fat body samples. We detected a ~ three-fold increase in levels of active/nuclear form SREBP (nSREBP) in *cg > shcircbabo(5,6,7,8S)-A* animals compared with controls (Fig. 4D, E). We conclude that SREBP is upregulated in *cg > shcircbabo(5,6,7,8S)-A* animals.

In addition, we explored the role of a collection of established lipid regulatory genes such as *Lsd-1/Lsd-2*, *Hsl*, and *bmm*, which are known to regulate lipid formation and lipolysis [44] in *circbabo(5,6,7,8S)*-depleted tissues. Firstly, we measured their expression levels and detected a significant reduction in *Lsd-1* levels (approximately ~ twofold). In contrast, *Lsd-2* and *bmm* exhibited increased expression (~ 1.5 fold and ~ 2.5 fold respectively). Level of the *Hsl* transcript remained unchanged (Additional file 5: Fig. S3A). These results indicate that the transcription of *Lsd-1*, *Lsd-2*, and *bmm* could be directly or indirectly regulated in *circbabo(5,6,7,8S)*-depleted tissues. Next, we introduced *UAS-bmm* or *UAS-shLsd-2* transgenes to the *cg > shcircbabo(5,6,7,8S)-A* background and examined the impact on LD accumulation phenotype (Additional file 5: Fig. S3D-E, S3J). As expected, overexpression of *bmm* enhances lipolysis, resulting in small LD size (Additional file 5: Fig. S3E, S3J), which is constant with previous reports [44]. Notably, overexpression of *bmm* in *circbabo(5,6,7,8S)*-depleted fat body effectively reduces LD accumulation (Additional file 5: Fig. S3D, S3J). *Lsd-2* has been reported to promote fat storage in lipid droplets [44]. Depletion of *Lsd-2* disrupts the lipid storage process, resulting in small LD size (Additional file 5: Fig. S3G, S3J). Simultaneous knockdown of *Lsd-2* and *circbabo(5,6,7,8S)* in the fat body reduces LD accumulation (Additional file 5: Fig. S3F, S3J). These results suggest that the lipolysis or lipid storage process remain mostly intact in *shcircbabo(5,6,7,8S)*-depleted flies, and that the LD accumulation phenotype in *shcircbabo(5,6,7,8S)*-depleted flies is unlikely due to dysfunction of lipolysis or lipid storage process. Given that promoting lipolysis or disrupting lipid storage in the *circbabo(5,6,7,8S)* depleted tissues can rescue the lipid accumulation defects (Additional file 5: Fig. S3B-G, S3J), these results further strengthen the notion that LD accumulation phenotype in *shcircbabo(5,6,7,8S)*-depleted flies is primarily due to alterations in lipogenesis.

To determine whether SREBP signaling is responsible for the LD accumulation and neurodegeneration phenotypes of *circbabo(5,6,7,8S)*-depleted flies, we first knocked down *SREBP* in the *cg > shcircbabo(5,6,7,8S)-A* flies and examined the impact on LD accumulation phenotype (Fig. 4F–K). Depletion of *SREBP* disrupts lipogenesis, resulting in small LD size and reduced TG storage (Fig. 4F, H, J, K). Simultaneous knockdown of *SREBP* and *circbabo(5,6,7,8S)* in the fat body effectively reduces LD accumulation (Fig. 4G, I, J, K). In addition, introducing one copy of the SREBP mutant allele, $SREBP^{\Delta 189}$ to the *cg > shcircbabo(5,6,7,8S)* background was able to suppress LD accumulation in fat body (Additional file 5: Fig. S3H-J) and partially rescue retinal degeneration (Additional file 5: Fig. S3K-R). Furthermore, since the aged neuronal *circbabo(5,6,7,8S)*-depleted flies display the most noticeable phenotypes, we reduced *SREBP* expression in the neurons of 30-day-old *GMR > shcircbabo(5,6,7,8S)-A* flies and assessed whether this would lessen the severity of photoreceptor cell loss. The results showed that the removal of *SREBP* in the eyes of *GMR > shcircbabo(5,6,7,8S)-A* flies improved neuronal integrity (Additional file 5: Fig. S3S-V). Moreover, we found that the reduction of *SREBP* in the *nSyb > shcircbabo(5,6,7,8S)-A* flies could also rescue the shortened lifespan phenotype (Additional file 5: Fig. S3W). Hence, our results strongly indicate that SREBP is a downstream effector of *circbabo(5,6,7,8S)* contributing

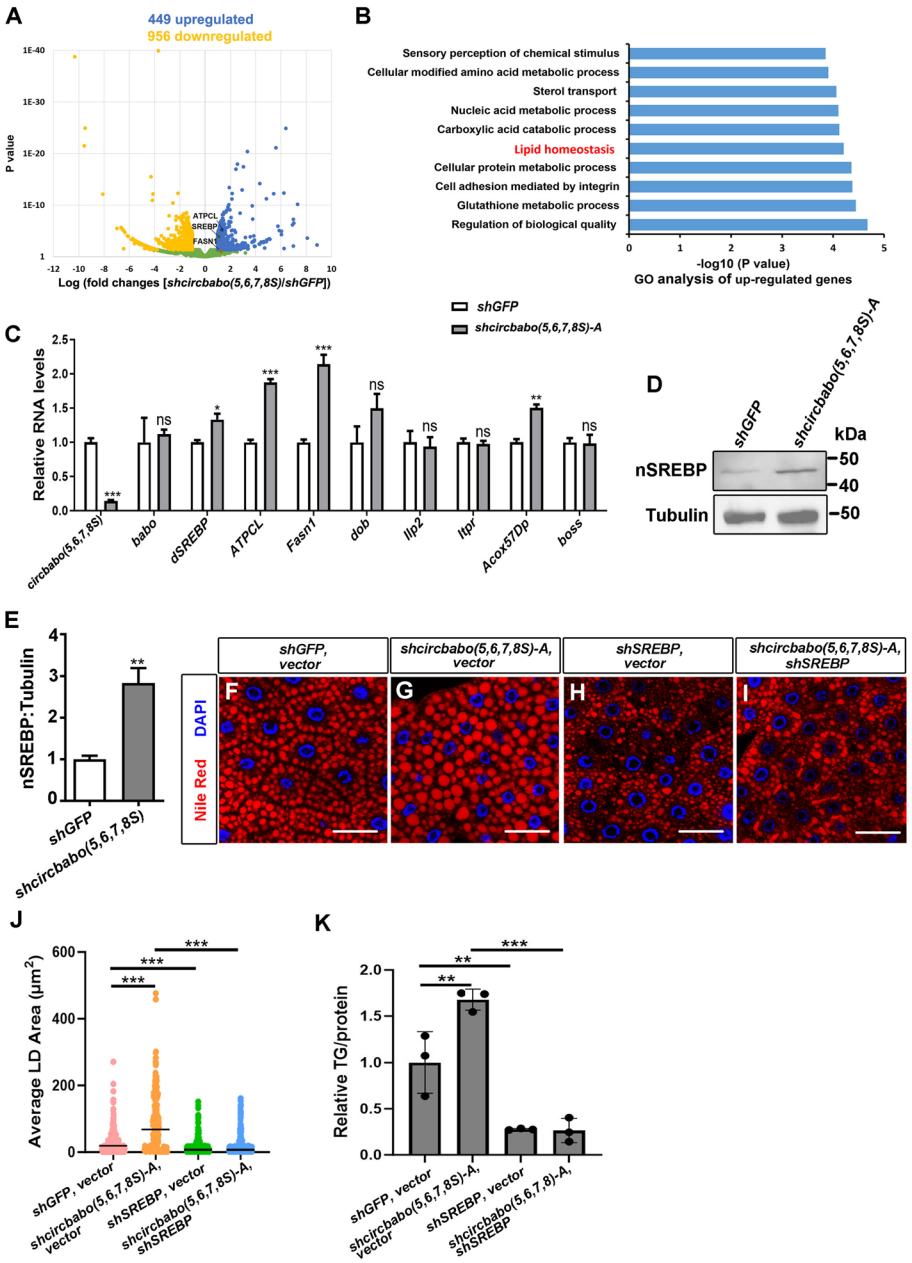

Fig. 4 Depletion of *circbabo(5,6,7,8S)* promotes the SREBP signaling pathway. **A** A volcano plot of gene expression profile of *cg-gal4 > shcircbabo(5,6,7,8S)-A* samples compared to control *cg-gal4 > shGFP* samples (fat body). Significantly upregulated genes (blue, $p \le 0.05$ and log2FC > 1), downregulated genes (yellow, $p \le 0.05$ and log2FC < −1), and genes with no change in expression (green) are shown. **B** Significantly upregulated genes were grouped into 10 categories based on Gene Ontology analysis. **C** Total RNA from the fat bodies of indicated genotypes were extracted and RT-qPCR was performed to quantify levels of select RNAs (Student's *t* test, $n = 3$, * $p < 0.05$; ** $p < 0.01$; *** $p < 0.001$; ns, non-significant). **D** Immunoblot shows levels of the nuclear form of SREBP (nSREBP) are elevated in the fat bodies of *cg > shcircbabo(5,6,7,8S)* flies. Tubulin serves as a loading control. **E** Quantification of results in **D** ($n = 3$). **F**–**I** Nile red was employed to stain LDs in the fat bodies of indicated genotypes. LDs accumulated in the fly fat bodies upon *circbabo(5,6,7,8S)* depletion (**F** and **G**). Knockdown of *SREBP* in the *shcircbabo(5,6,7,8S)* background reduces the degree of LD accumulation (compare **G** and **I**). Scale bar, 50 μm. **J** Quantification of LD size in **F**, **G**, **H**, and **I** (one-way ANOVA with Turkey post hoc test, $n = 3$, *** $p < 0.001$). **K** TG levels in fat bodies of genotypes similar to those in **F**, **G**, **H**, and **I** were measured and normalized (one-way ANOVA with Turkey post hoc test, $n = 3$, ** $p < 0.01$; *** $p < 0.001$)

to the LD accumulation and neurodegeneration phenotypes in *circbabo(5,6,7,8S)*-depleted flies.

circbabo(5,6,7,8S) encodes a functional protein

While circRNAs were initially thought to be non-coding RNAs, recent findings suggest that select circRNAs have the potential to be translated into functional proteins [32, 33, 45, 46]. We noticed that *circbabo(5,6,7,8S)* contains a potential open reading frame (ORF) (see Additional file 1: Table S1 for the highlighted sequence), which includes two closely located start codons and one common stop codon. The hypothetical protein product consists of 350 amino acids, overlapping with the C-terminus of the babo protein and encompassing the GS and the kinase domains of babo (Fig. 5A). We named the hypothetical protein product as circbabo(5,6,7,8S)-p. To test the protein-coding potential of *circbabo(5,6,7,8S)*, we performed RNA immunoprecipitation using the ribosomal protein RpL22, which is an essential ribosomal protein for translation. Lysates were prepared from *Drosophila* SL2 cells stably expressing TAP-RpL22 or a control TAP tag only, and immunoprecipitation assays using IgG-conjugated agarose beads. Total RNA was extracted from immuno-purified samples, levels of various RNAs were measured and compared with controls. We found that similar to protein-coding mRNAs *Rp49* and *Reaper*, *circbabo(5,6,7,8S)* was significantly enriched in the RpL22 pull-down sample compared to the control, indicating protein-coding potential (Additional file 6: Fig. S4A). To validate this hypothesis, we generated a *circbabo(5,6,7,8S)* transgene with a 3XFlag epitope tag positioned immediately upstream of the putative stop codon in the ORF of *circbabo(5,6,7,8S)* (Fig. 5B). Lysate from SL2 cells stably expressing the *circbabo(5,6,7,8S)-Flag* transgene was subjected to immunoprecipitation using the anti-Flag antibody, and both cell lysates and immuno-purified anti-Flag complexes were subjected to immunoblot. Two Flag-tagged protein bands (p1 and p2) were detected in both cell lysate and immuno-purified anti-Flag complexes, presumably due to the presence of two closely spaced initiation codons in the putative ORF (Fig. 5C, D). We note that levels of the second product (p2) are weaker than p1, consistent with the notion that the first AUG codon primarily serves as the main translation initiation site [47]. However, we cannot exclude the possibility that p2 could also be a degradation product of p1. To confirm that the Flag-tagged protein products are derived from *circbabo(5,6,7,8S)*, immuno-purified anti-Flag samples were subjected to mass spectrometry. We detected 7 distinct peptides originating from the putative *circbabo(5,6,7,8S)* ORF (Fig. 5D, Additional file 7: Table S3), thereby demonstrating the protein-coding capability of *circbabo(5,6,7,8S)*. In the *circbabo(5,6,7,8S)–3XFlag* transgene employed in Fig. 5B, the stop codon is located downstream of the initiation codon; therefore, we could not exclude the possibility that the protein product could be derived from the linear transcript. To rule out this possibility, we generated a second *3XFlag-stop-circbabo(5,6,7,8S)* transgene in which the stop codon is positioned upstream of the initiation codon, and the backspliced junction is positioned within the ORF, while still maintaining the circRNA

(See figure on next page.)

Fig. 5 *circbabo(5,6,7,8S)* encodes a functional protein. **A** Schematic of the babo and circbabo-p proteins. Positions of the LB (ligand bind), TM (transmembrane), GS (TTSGSGSG sequence), and kinase domains are shown. **B** Schematic of a *circbabo(5,6,7,8S)* minigene driven by the *metallothionein* promoter. The ORF and the corresponding UTR are shown in green and blue, respectively. Two candidate start codons and one stop codon are noted. A 3X FLAG epitope tag-coding sequence was placed immediately upstream of the putative stop codon. **C** SL2 cells were transfected with empty vector or the *circbabo(5,6,7,8S)* minigene described in **B**. Cell lysates were subject to anti-Flag immunoprecipitation. Two Flag-tagged protein bands (p1 and p2) were detected in cell lysates and enriched in immunopurified samples. p2 could be either a product derived from the shorter ORF or a degradation product of p1. **C'** is the long exposure of **C**. **D** Lysate from stably transfected SL2 cells carrying the constructs described in **B** was subjected to anti-Flag IP followed by mass spectrometry. Seven independent peptides (in green) derived from circbabo(5,6,7,8S)-p were identified. **E–H** Flies carrying the fat body-specific *cg-Gal4* driver were crossed to *UAS-shcircbabo(5,6,7,8S)-A* or control *UAS-shGFP* flies together with the empty vector or the *UAS-Flag-circbabo(5,6,7,8S)-p* transgene. Nile red and DAPI staining, respectively, labels neutral lipids and nuclei in fat bodies of the indicated genotypes. Expression of *Flag-circbabo(5,6,7,8S)-p* in the *shcircbabo(5,6,7,8S)* background rescues the LD accumulation phenotype. Scale bar, 20 μm. **I** Levels of Flag-circbabo(5,6,7,8S)-p protein were measured by immunoblot. **J** Quantification of LD size in **E**, **F**, **G**, and **H** (one-way ANOVA with Turkey post hoc test, $n = 5$, *** $p < 0.001$; ns, non-significant). **K** TG levels in a similar set of samples as in **E**, **F**, **G**, and **H** (fat bodies) were measured and normalized (one-way ANOVA with Turkey post hoc test, $n = 3$, *** $p < 0.001$; ns, non-significant). **L–N** Flies carrying the *GMR-Gal4* driver were crossed to *UAS-shcircbabo(5,6,7,8S)-A* or control *UAS-shGFP* flies together with the empty vector or the *UAS-Flag-circbabo(5,6,7,8S)-p* transgene. The eyes of 30-day-old flies with the indicated genotypes were analyzed by TEM. The photoreceptor cell loss phenotype was rescued by introducing the *Flag-circbabo(5,6,7,8S)-p* transgene in the *shcircbabo(5,6,7,8S)-A* genetic background. Scale bar, 5 μm. **O** Quantification of the number of intact photoreceptors in each ommatidium from flies with the indicated genotypes of **L–N**. Different number of **L** = 19, **M** = 32, **N** = 19 ommatidia were counted. **P** Flies carrying the pan neuronal *nSyb-Gal4* driver were crossed to *UAS-shcircbabo(5,6,7,8S)-A* or control *UAS-shGFP* flies together with the empty vector or the *UAS-Flag-circbabo(5,6,7,8S)-p* transgene. The lifespan of flies of select genotypes is shown (*n* represents number of groups for each genotype, 16–20 flies for each group. *shGFP, vector* = 10; *shcircbabo(5,6,7,8S)-A, vector* = 10; *shGFP, Flga-circbabo(5,6,7,8S)-p* = 8; *shcircbabo(5,6,7,8S), Flag-circbabo(5,6,7,8S)-p* = 8)

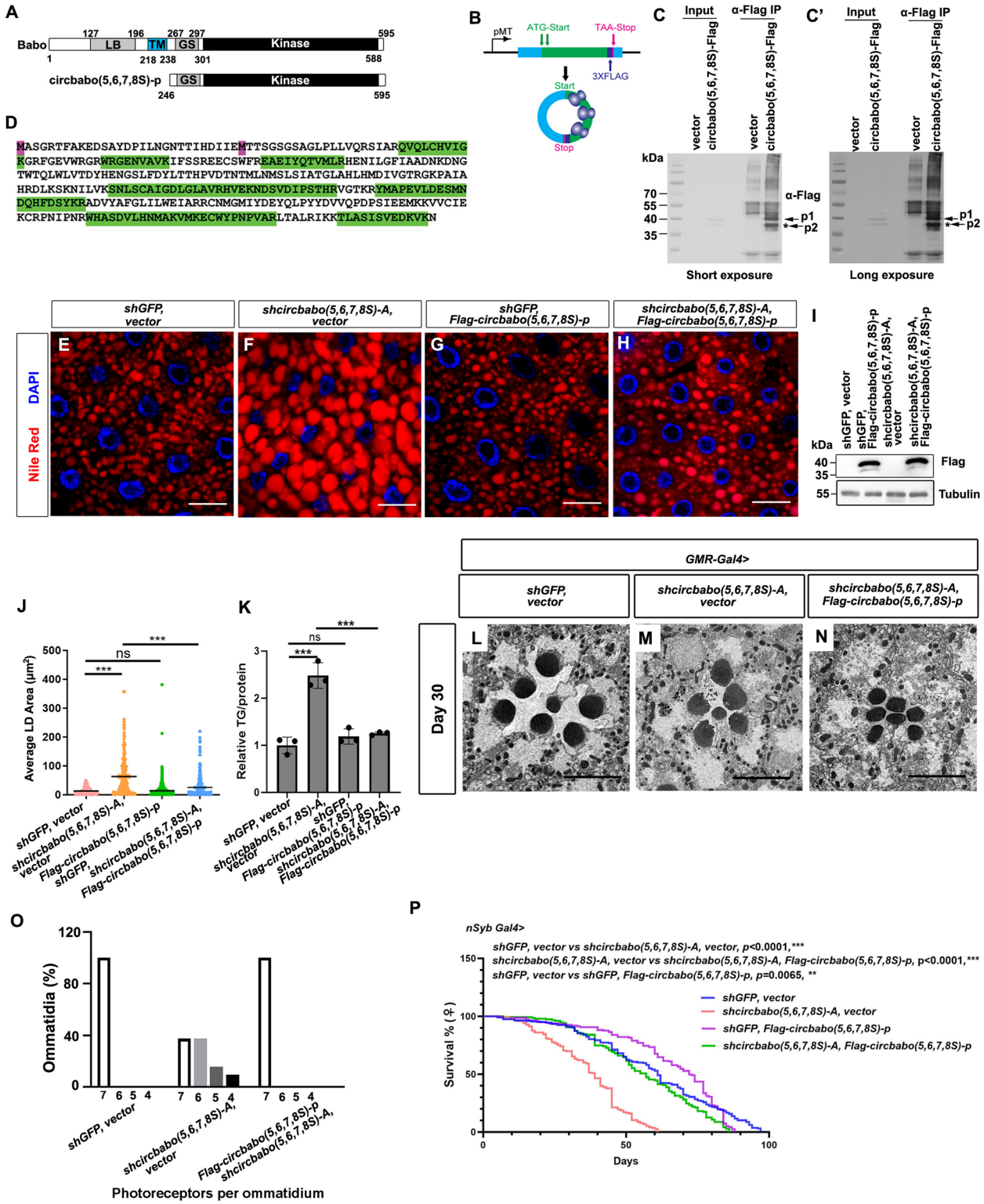

Fig. 5 (See legend on previous page.)

configuration (Additional file 6: Fig. S4B). Upon introducing this construct into S2-TM cells, we were able to detect two Flag-tagged protein bands in immuno-purified Flag-tagged protein complexes, and the sizes are comparable to p1 and p2 in *circbabo(5,6,7,8S)−3XFlag* expressing cells (Additional file 6: Fig. S4C). Thus, we conclude that *circbabo(5,6,7,8S)* has protein-coding potential, at least in the transgene setting.

To uncover the biological function of the circRNA-encoded protein circbabo(5,6,7,8S)-p, we examined whether circbabo(5,6,7,8S)-p can rescue the phenotypes elicited by *circbabo(5,6,7,8S)* depletion in vivo. To this end, we generated transgenic flies carrying the protein-coding sequence of Flag-circbabo(5,6,7,8S)-p under the control of UAS. Expression of Flag-circbabo(5,6,7,8S)-p in fat body rescued the enlarged LD size and TG over-storage phenotypes of *cg > shcircbabo(5,6,7,8S)* animals (Fig. 5E–K). In addition, the defective ommatidium structure in 30-day-old *circbabo(5,6,7,8S)*-depleted flies driven by *GMR-Gal4* was also rescued by Flag-circbabo(5,6,7,8S)-p (Fig. 5L-O). Lastly, expression of Flag-circbabo(5,6,7,8S)-p in neurons using *nSyb-Gal4* rescued the shortened lifespan resulting from the depletion of *circbabo(5,6,7,8S)* (Fig. 5P). Taken together, these data solidify the notion that *circbabo(5,6,7,8S)* encodes a functional protein.

circbabo(5,6,7,8S) regulates the TGF-β signaling pathway

Our data show that expression of circbabo(5,6,7,8S)-p or depletion of SREBP rescues the phenotypes elicited by *circbabo(5,6,7,8S)* depletion. We first set out to examine whether there is any physical interaction between circbabo(5,6,7,8S)-p and SREBP. Our immunoprecipitation assay failed to detect such interactions (Additional file 8: Fig. S5A). In addition, our analysis reveals that circbabo(5,6,7,8S)-p is primarily localized in the cytoplasm, thus it is unlikely to directly regulate transcription (Additional file 8: Fig. S5B). We conclude that *circbabo(5,6,7,8S)* may indirectly regulate the SREBP signaling pathway to impact lipid metabolism.

Babo is the type I receptor for the activin-like ligands of the TGF-β signaling pathway in *Drosophila* [48]. Ligand binding to the type I receptor babo induces the formation of a receptor complex consisting of both babo and type II receptors (put or wit). The constitutively active type II receptors in turn phosphorylate babo, ultimately leading to Smad phosphorylation. Subsequently, phosphorylated Smad binds to Medea and translocates to the nucleus to initiate a transcriptional response [49]. Previous studies have shown that ectopic activation of the babo-dependent TGF-β signaling pathway in the fat body leads to lipid accumulation and mitochondrial dysfunction [39]. Since circbabo(5,6,7,8S)-p is a truncated form of babo, we hypothesized that *circbabo(5,6,7,8S)* may regulate lipid metabolism by interfering with the TGF-β signaling pathway. To test this hypothesis, we first conducted KEGG pathway analysis using the RNA-seq data from *cg > shcircbabo(5,6,7,8S)-A* and the *cg > shGFP* control animals. Our analysis revealed that the TGF-β pathway ($p = 0.041$) is among the processes with enrichment of differentially expressed genes in *cg > shcircbabo(5,6,7,8S)-A* flies (Additional file 8: Fig. S5C). Indeed, immunoblot revealed a ~ fivefold increase in levels of p-Smad in *circbabo(5,6,7,8S)*-depleted fat body cells compared with controls (Fig. 6A), reflecting enhanced activation of TGF-β signaling. In contrast, we detected a ~ 25% reduction in levels of p-Smad in Flag-circbabo(5,6,7,8S)-p overexpressing fat body cells compared with controls (Fig. 6B). As a positive control for TGF-β pathway activation, overexpression of babo Q302D, a constitutively active form of babo, induced a prominent increase in levels of p-Smad in the fat body (Fig. 6B). In addition, consistent with previous reports, forced expression of babo Q302D in fat body cells also led to lipid accumulation (Additional file 9: Fig. S6A, B, E). Interestingly, depletion of *SREBP* in babo Q302D-expressing cells could rescue the lipid accumulation phenotypes, suggesting that SREBP acts downstream of TGF-β signaling (Additional file 9: Fig. S6B-E). Furthermore, forced expression of babo Q302D in the *Drosophila* eyes could lead to LD formation in the ommatidia (Additional file 9: Fig. S6F-G). Taken together, our analyses indicated that the TGF-β signaling pathway regulates lipid metabolism in both fat body and neurons.

Our data suggest that *circbabo(5,6,7,8S)* regulates the TGF-β signaling pathway. Since circbabo(5,6,7,8S)-p is presumably a soluble cytoplasmic fragment of babo, it may act in a dominant negative fashion by competing with babo for limiting components required for the activation of TGF-β signaling, thereby interfering with babo-dependent TGF-β signaling. To test this hypothesis, we first examined whether circbabo(5,6,7,8S)-p could associate with core components of babo-dependent TGF-β signaling pathway. We expressed Flag-tagged circbabo(5,6,7,8S)-p and HA-tagged babo in SL2 cells. Reciprocal co-immunoprecipitation assays confirmed that circbabo(5,6,7,8S)-p interacts with babo (Fig. 6C). We also confirmed the interaction between babo and put (Additional file 10: Fig. S7), consistent with previous report showing that babo associates with put to form a heterodimeric receptor complex [50]. Interestingly, we found that Flag-circbabo(5,6,7,8S)-p co-precipitated with put-HA, but not with Smad-HA (Fig. 6D, E), suggesting that either circbabo(5,6,7,8S)-p does not interact with Smad, or the interaction is weak/transient and beyond detection limits. Since babo and put interact each other,

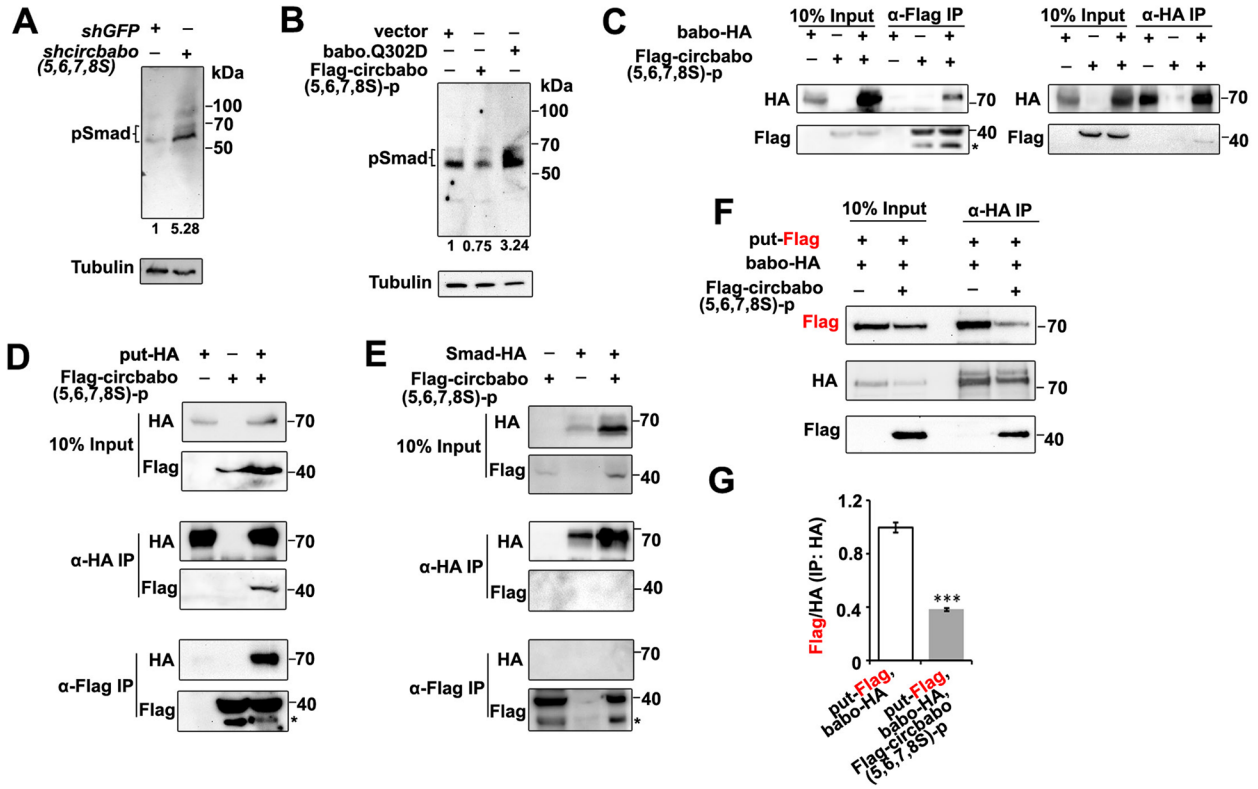

Fig. 6 circbabo(5,6,7,8S)-p dampens TGF-β signaling by interfering with babo/put receptor heterodimerization. **A** Flies carrying the *cg-Gal4* driver were crossed to *shGFP* (control) or *shcircbabo(5,6,7,8S)* flies. Immunoblot analysis of fat bodies of the indicated genotypes shows that levels of pSmad are elevated upon *circbabo(5,6,7,8S)* depletion. Tubulin serves as a loading control. **B** Levels of pSmad are decreased in the fat bodies of *cg > Flag-circbabo(5,6,7,8S)-p* flies, and elevated in fat bodies overexpressing babo.Q302D. Tubulin serves as a loading control. **C** Flag tagged circbabo(5,6,7,8S)-p could pull-down HA tagged babo. Various combinations of expression constructs for Flag-tagged circbabo(5,6,7,8S)-p and HA-tagged babo were transfected into S2 cells. Both 10% of cell lysates and immuno-purified HA and Flag complexes were analyzed by immunoblot. **D** Flag tagged circbabo(5,6,7,8S)-p could pull-down HA tagged put. Various combinations of expression constructs for Flag-tagged circbabo(5,6,7,8S)-p and HA-tagged put were transfected into S2 cells. Both 10% of cell lysates and immuno-purified HA and Flag complexes were analyzed by immunoblot. **E** circbabo(5,6,7,8S)-p and Smad did not interact with each other. Various combinations of expression constructs for Flag-tagged circbabo(5,6,7,8S)-p and HA-tagged Smad were transfected into S2 cells. Both 10% of cell lysates and immuno-purified HA and Flag complexes were analyzed by immunoblot. **F** circbabo(5,6,7,8S)-p interferes with babo/put receptor heterodimerization. Various combinations of expression constructs for Flag-tagged circbabo(5,6,7,8S)-p, Flag-tagged put and HA-tagged babo were transfected into S2 cells. Both 10% of cell lysates and immuno-purified HA complexes were analyzed by immunoblot. **G** Quantification of the ratio of Flag-put/HA-babo intensity in the immuno-purified HA complexes as shown in **F**. The experiment has been repeated 3 times (student t-test, ***$p < 0.001$)

and both can associate with circbabo(5,6,7,8S)-p, we posited that circbabo(5,6,7,8S)-p might interfere with TGF-β signaling by weakening the interaction between put and babo. To test this, we co-expressed in SL2 cells babo-HA and put-Flag with or without Flag-circbabo(5,6,7,8S)-p, performed IP using an anti-HA antibody, and measured levels of put-Flag in the immuno-purified babo-HA complexes. Indeed, in the presence of Flag-circbabo(5,6,7,8S)-p, the amount of put that co-immunoprecipitated with babo was significantly reduced (Fig. 6F, G). Taken together, our analyses show that circbabo(5,6,7,8S)-p may dampen the interaction between the type II receptor put and type I receptor babo, thereby fine-tuning the output of the TGF-β signaling pathway.

The ROS/JNK/SREBP cascade regulates lipid homeostasis and neuronal integrity in *circbabo(5,6,7,8S)*-depleted flies

Previous studies have shown that TGF-β signaling can inhibit various mitochondrial functions, including oxidative phosphorylation, glycolytic capacity, and respiratory capacity in different organisms. For example, activation of TGF-β signaling autonomously leads to decreased ATP production and an excess of ROS in cells [39, 51, 52]. Consistent with previous reports, forced expression of babo Q302D in the fat body cells led to a marked decrease in ATP levels, which reflects mitochondrial dysfunction (Additional file 11: Fig. S8A). Next, we measured ROS levels in the fat body using the ROS-related fluorescent dye, 2',7'-dichlorodihydrofluorescein (DCF), and

detected higher levels of ROS in fat body expressing babo Q302D than in controls, further confirming that aberrant activation of TGF-β signaling led to mitochondrial dysfunction (Additional file 11: Fig. S8B-D). Since depletion of *circbabo(5,6,7,8S)* led to enhanced TGF-β signaling, we hypothesized that it may also cause mitochondrial dysfunction. Indeed, we found that the depletion of *circbabo(5,6,7,8S)* in the fat body resulted in reduced ATP levels and elevated ROS, as shown by increased DCF fluorescence intensity compared with control animals (Additional file 11: Fig. S8A, E, F, H). In addition, we employed the oxidative stress reporter *GstD1*-GFP to quantify ROS levels in *circbabo(5,6,7,8S)*-depleted tissues [53]. This analysis revealed that fat body-specific depletion of *circbabo(5,6,7,8S)* led to elevated *GstD1*-GFP reporter activity compared with control (Fig. 7A, B, D), reflecting ROS over-accumulation.

ROS affects the homeostasis of intracellular lipid metabolism in both *Drosophila* and mammals [27, 54, 55]. Expression of *hSOD1*, which encodes an enzyme that removes ROS, using the fat body driver *cg-GAL4* eliminated ROS in *circbabo(5,6,7,8S)*-depleted cells (Additional file 11: Fig. S8G, H; Fig. 7C, D), and also reduced LD accumulation (Fig. 7E–G, I, J). In addition, expression of *hSOD1* in *circbabo(5,6,7,8S)*-depleted eyes using *GMR-GAL4* partially rescues the eye degeneration and LD accumulation defects (Fig. 7K-M, O, Additional file 12: Fig.S9). Furthermore, the shortened lifespan phenotype elicited by neuron-specific *circbabo(5,6,7,8S)* depletion was rescued upon *hSOD1* expression (Fig. 7P). Taken together, our data show that the depletion of *circbabo(5,6,7,8S)* induces ROS production, which contributes to lipid accumulation and neuronal degeneration.

It has been reported that ROS activates transcription factors such as FoxO and NF-κB/Rel, and the JNK signaling pathway, which in turn impact SREBP activity [27, 56–58]. To determine whether these factors play a role in the LD accumulation phenotype in *circbabo(5,6,7,8S)*-depleted flies, we knocked down *FoxO*, *JNK,* or *Rel* in the *cg > shcircbabo(5,6,7,8S)-A* background, and examined the impact on LD formation. We found that removal of bsk (the homolog of JNK in *Drosophila*) is sufficient to reduce lipid accumulation in the fat body of *circbabo(5,6,7,8S)*-depleted flies (Fig. 7H–J), while depletion of Rel or FoxO had no impact (Additional file 13: Fig. S10). In addition, we performed immunoblot to measure levels of JNK in the fat body lysate from the 3rd *instar* larvae. We found that *circbabo(5,6,7,8S)*-depletion or *babo Q302D* expression led to notable elevation of total JNK levels (Additional file 14: Fig. S11). To investigate the role of JNK in the neurodegeneration phenotype of *circbabo(5,6,7,8S)*-depleted flies, we depleted *bsk* in the *GMR > shcircbabo(5,6,7,8S)-A* background. We found that the eye degeneration phenotype in *circbabo(5,6,7,8S)*-depleted flies was partially rescued by *bsk* knockdown (Fig. 7N,O). Additionally, the lifespan was extended by depletion of *bsk* in *nSyb > shcircbabo(5,6,7,8S)-A* flies (Fig. 7P). All those data confirm that JNK signaling contributes to the LD accumulation and retina degeneration in *circbabo(5,6,7,8S)*-depleted flies. Taken together, our analyses show that *circbabo(5,6,7,8S)* depletion enhances TGF-β signaling and promotes the ROS/JNK/SREBP cascade to impact lipid homeostasis and neuronal health.

Discussion

In this study, we identified a circRNA derived from the *babo* locus, *circbabo(5,6,7,8S)*, which is highly abundant in the fat body cells of *Drosophila*. We show that fat body-specific depletion of *circbabo(5,6,7,8S)* causes LD accumulation and increased TG contents. In addition, despite its relatively lower expression in the brain than in fat body, *circbabo(5,6,7,8S)* is essential for neuronal health. Specifically, *circbabo(5,6,7,8S)*-depletion leads to a shortened lifespan and photoreceptor cell degeneration accompanied by LD accumulation in retinas, a phenotype that manifests predominantly in young flies. Regarding

(See figure on next page.)

Fig. 7 Reducing levels of ROS, JNK, or SREBP in *circbabo(5,6,7,8S)*-depleted flies rescues the LD accumulation and neurodegeneration phenotypes. **A–C** Fat bodies carrying the *GstD1-GFP* reporter and expressing the indicated transgenes under the control of *cg-Gal4* were imaged to visualize GFP (green). *circbabo(5,6,7,8S)* depletion led to increased levels of *GstD1-GFP*. This phenotype can be rescued by introducing the *hSOD1* transgene. Scale bar, 20 μm. **D** Quantification of GFP fluorescence intensity in **A**, **B**, and **C** (one-way ANOVA with Turkey post hoc test, $n = 3–4$, ** $p < 0.01$; *** $p < 0.001$). **E–H** Various combinations of the indicated transgenes were expressed under the control of *cg-Gal4*. Nile red and DAPI were employed to label lipid droplets and nuclei, respectively. Overexpression of *hSOD1* or knockdown of *bsk* rescued the LD accumulation phenotype in *cg > shcircbabo(5,6,7,8S)* flies. (**I**) Quantification of LD size in **E**, **F**, **G**, and **H** (one-way ANOVA with Turkey post hoc test, $n = 5$, * $p < 0.05$; *** $p < 0.001$; ns, non-significant). **J** TG levels in a similar set of samples as in **E**, **F**, **G**, and **H** were measured and normalized (one-way ANOVA with Turkey post hoc test, $n = 3$, * $p < 0.05$; ** $p < 0.01$). **K–N** The eyes of 30-day-old flies carrying the indicated combinations of transgenes driven by *GMR-Gal4* were analyzed with TEM. The photoreceptor cell loss phenotype elicited by the depletion of *circbabo(5,6,7,8S)* was rescued by *hSOD1* overexpression or *bsk* depletion. Scale bar, 5 μm. **O** Quantification of the number of intact photoreceptors in each ommatidium from flies with the indicated genotypes of **K–N**. Different number of (**K** = 19, **L** = 32, **M** = 11, **N** = 11) ommatidiawere counted. **P** Lifespan of flies carrying the indicated combinations of transgenes driven by the pan neuronal *nSyb-Gal4* driver is shown (*n* represents number of groups for each genotype, 15–20 flies for each group. *shGFP, vector* = 10; *shcircbabo(5,6,7,8S)-A, vector* = 10; *shcircbabo(5,6,7,8S), hSOD1* = 9; *shcircbabo(5,6,7,8S), shbsk* = 8)

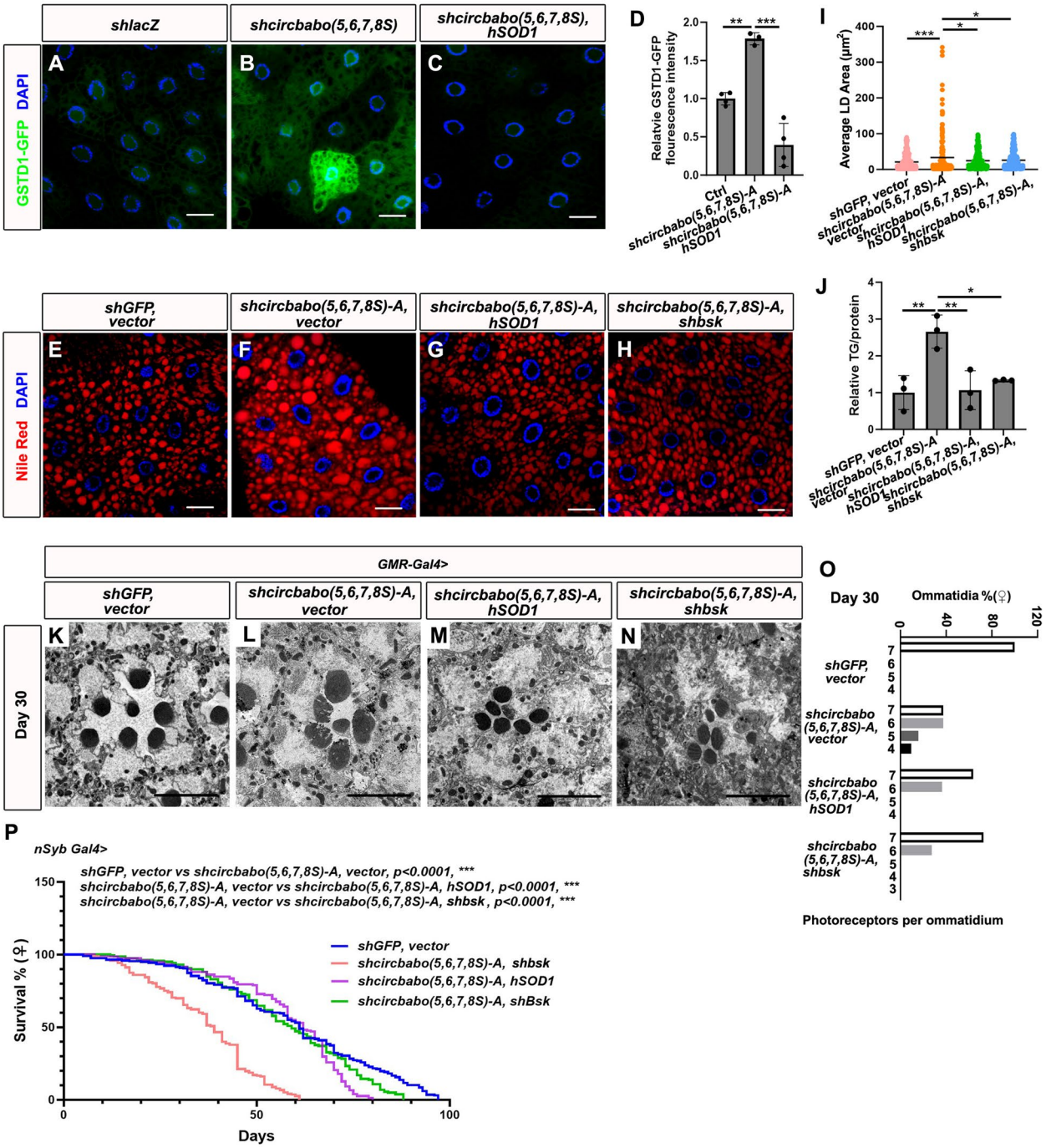

Fig. 7 (See legend on previous page.)

the molecular mechanism underlying *circbabo(5,6,7,8S)* function, we provide evidence that *circbabo(5,6,7,8S)* encodes a functional protein and regulates TGF-β signaling by interfering with babo/put heterodimeric receptor assembly, consequently impairing downstream Smad protein phosphorylation. In addition, depletion of *circbabo(5,6,7,8S)* leads to enhanced activation of TGF-β signaling, resulting in mitochondrial dysfunction and increased ROS levels. Lastly, we show that ROS promotes the expression of lipogenesis genes through the JNK/SREBP signaling cascade, leading to enhanced lipid synthesis and accumulation in cells (Fig. 8). Thus, our study establishes a regulatory role for *circbabo(5,6,7,8S)* in lipid metabolism and neuronal integrity.

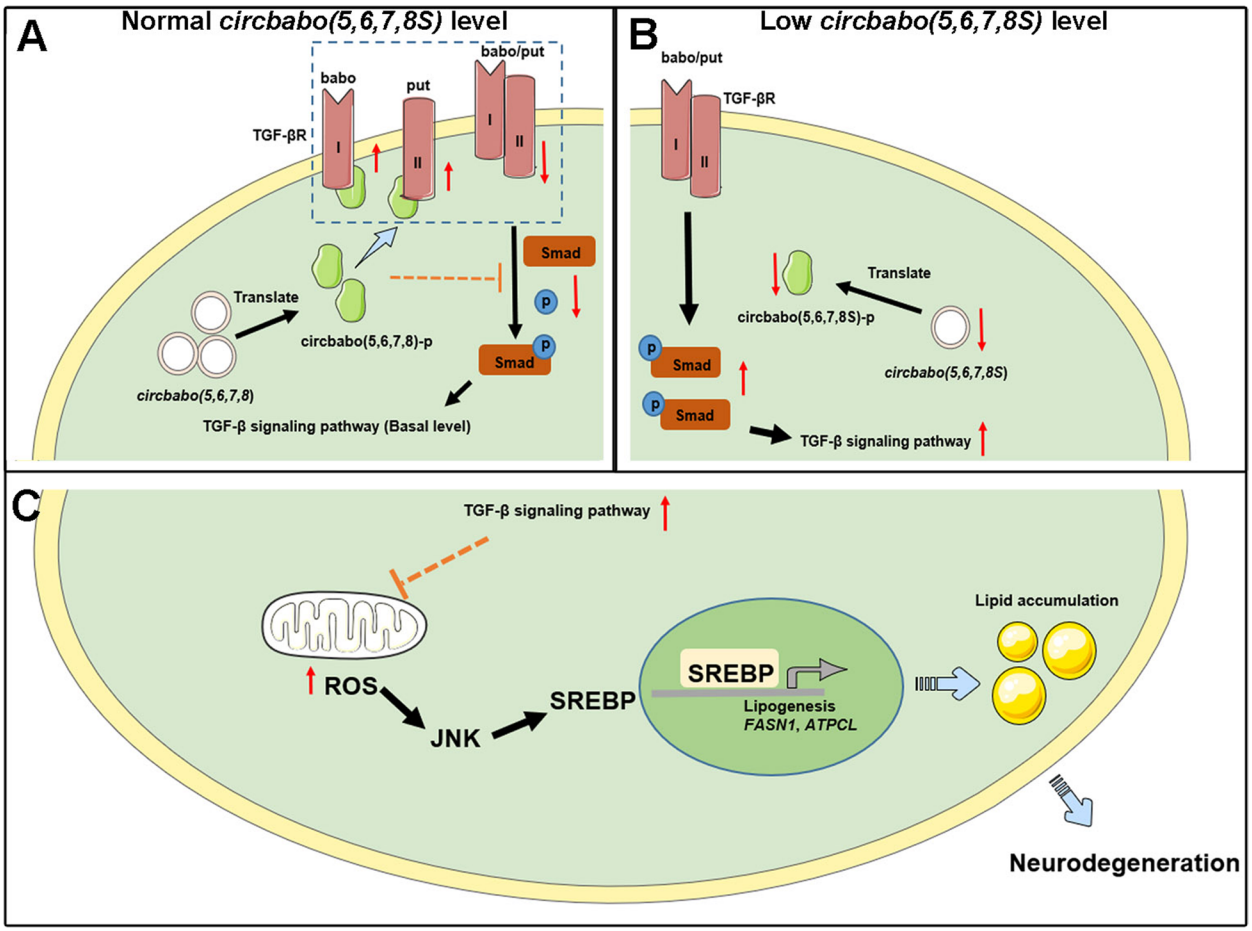

Fig. 8 A diagram depicting the role of *circbabo(5,6,7,8S)* in lipid metabolism. **A** With normal levels of *circbabo(5,6,7,8S)* expression, *circbabo(5,6,7,8S)* is translated into the circbabo(5,6,7,8S)-p protein, which interferes with the babo/put receptor heterodimerization, thereby dampening the phosphorylation of Smad and reducing the output of TGF-β signaling. **B** Upon *circbabo(5,6,7,8S)* depletion, Smad phosphorylation/activation is enhanced, leading to an increase in the output of TGF-β signaling. **C** TGF-β signaling inhibits mitochondrial function, leading to an increase in ROS levels. ROS in turn triggers JNK-SREBP signaling, which promotes the transcription of lipogenesis genes (*FASN1*, *ATPCL*), leading to lipid accumulation

Our study revealed that *circbabo(5,6,7,8S)* can encode a functional protein, which is essentially a truncated form of babo (Fig. 5A–D). Since there are no new amino acid sequences in circbabo(5,6,7,8S)-p that can differentiate from babo, it would be challenging to detect the endogenous *circbabo(5,6,7,8S)*-derived proteins by mass spectrometry. In addition, our attempts to insert epitope tags into the exons that give rise to endogenous circbabo(5,6,7,8S) were unsuccessful, possibly because this modification would result in the addition of exogenous amino acid sequences to the endogenous babo protein, which may cause a growth disadvantage and prevent the formation of SL2 cell clones. Therefore, it remains unclear whether endogenous circbabo(5,6,7,8S)-p can be produced in vivo. Nonetheless, our functional analyses revealed that expression of circbabo(5,6,7,8S)-p rescued the LD accumulation, neurodegeneration, and shortened lifespan phenotypes elicited by *circbabo(5,6,7,8S)* depletion (Fig. 5E–P). Thus, we propose that circbabo(5,6,7,8S)-p is a functional module of *circbabo(5,6,7,8S)* in regulating lipid metabolism and neuronal integrity.

Although select circRNAs encode proteins and perform distinct functions from their linear counterparts [45, 50, 59, 60], recent studies showed that some circRNAs participate in the same biological processes and even exert dominant-negative effects on proteins encoded by their linear sibling mRNAs [32, 59, 61]. Here, we found that *circbabo(5,6,7,8S)* and *babo* are derived from the same pool of pre-mRNAs, yet they display opposing functions, as depletion of *babo* and *circbabo(5,6,7,8S)*, respectively, leads to a reduction and an increase in lipid accumulation. This is consistent with our findings showing that *circbabo(5,6,7,8S)* encodes a truncated form of babo protein, which exerts a dominant negative effect on babo by competing with babo for limiting core components

of TGF-β signaling, such as put, thereby inhibiting the TGF-β signaling (Fig. 6A, B, F, G). Thus, the *babo* gene locus appears to produce multiple protein isoforms to achieve more precise control of TGF-β signaling through the canonical and back-splicing events. This would minimize the necessity of evolving additional transcription initiation sites at the *babo* locus or protease cleavage sites in the babo protein, and represents an efficient strategy to achieve precise fine-tuning of the activity of proteins or the output of a given biological pathway/process.

Ectopic activation of the SREBP signaling pathway, which promotes lipid synthesis, is responsible for the lipid metabolism phenotype in *circbabo(5,6,7,8S)*-depleted fat body cells (Fig. 4, S3). However, we did not detect a direct interaction between circbabo(5,6,7,8S)-p and SREBP, implying that circbabo(5,6,7,8S)-p may indirectly regulate the SREBP signaling pathway (Additional file 8: Fig. S5A). Indeed, overactive TGF-β signaling can lead to mitochondrial dysfunction, resulting in increased ROS generation and reduced ATP production (Fig. 7A–D, Additional file 11: Fig. S8). Our analysis revealed that hSod1-mediated clearance of ROS rescued the LD accumulation and neurodegeneration phenotypes (Fig. 7E–P, Additional file 12: Fig.S9), consistent with previous reports showing that ROS activates the SREBP signaling in *Drosophila* [27].

We note that the overexpression of *circbabo(5,6,7,8S)* and *Flag-circbabo(5,6,7,8S)-p* extend the lifespan of fruit flies. This lifespan extension effect could be a result of the inhibitory effect of *circbabo(5,6,7,8S)* on the TGF-β signaling pathway (Figs. 6B and 8). Reduced TGF-β signaling has been reported to extend longevity by modulating insulin signaling [62] and autophagy process [63]. Further investigation is needed to elucidate the detailed molecular mechanisms of *circbabo(5,6,7,8S)* in regulating lifespan.

In most cases, the over-produced lipid in neurons can be further transported to the glia with the help of monocarboxylate transporters (MCTs), fatty acid transport proteins (FATPs), and apolipoproteins (APOE) [64–66]. In the retinas of *circbabo(5,6,7,8S)* depletion flies, we found that enhanced lipogenesis causes LD formation predominantly in neurons, and only a small amount of LDs are detected in the glia (Additional file 3: Fig. S2A-G). This could be due to that the LD accumulation phenotype of *circbabo(5,6,7,8S)*-depleted flies is relatively weak; therefore, there are not enough lipids to be transported to the glia. In addition, it has reported that activation of TGF-β signaling in neurons results in the repression of APOE RNA and protein levels [67]. Thus, enhanced-activation of TGF-β signaling in *circbabo(5,6,7,8S)*-depleted neurons may impact the lipid transport system between neurons and glia. The formation of LDs in glial cells is crucial for protecting neurons under stress conditions [68]. In contrast, LD accumulation in neurons contributes to pathology. For example, loss of the lipolysis gene *ATGL-1* / *LID-1* causes LD accumulation in neurons and neurodegeneration in *C. elegans* [13]. Thus, a delicate balance between lipolysis and lipogenesis is critical for regulating neuronal lipid homeostasis and health.

Conclusions

The *circbabo(5,6,7,8S)* encoded protein circbabo(5,6,7,8S)-p regulates the TGF-β signaling pathway by interfering with the assembly of babo/put heterodimeric receptor complex. Depletion of *circbabo(5,6,7,8S)* leads to enhanced activation of TGF-β signaling and compromised mitochondrial function. Moreover, dysregulation of the ROS/JNK/SREBP signaling cascade is responsible for the LD accumulation, neurodegeneration, and shortened lifespan phenotypes elicited by *circbabo(5,6,7,8S)* depletion. Thus, we conclude that the protein-coding circRNA *circbabo(5,6,7,8S)* is a regulator of lipid metabolism and neuronal integrity.

Methods

Molecular cloning

To knock down circRNAs, shRNA constructs were generated using the Valium 20 parental vector as previously described [32]. To overexpress *circbabo(5,6,7,8S)* in SL2 cells, a DNA fragment containing the *circbabo(5,6,7,8S)*-generating exons was amplified by PCR, and cloned into the Hy_pMT Laccase2 MCS exon vector using AgeI and SacI [69]. Overexpression construct for *circbabo(5,6,7,8S)* in flies: a DNA fragment containing the *circbabo(5,6,7,8S)* and flanking *Laccase2* intronic sequences was purified from the Hy_pMT Laccase2-*circbabo(5,6,7,8S)* by sequential treatment of XhoI, T4 DNA polymerase, and NotI and inserted into the pUAST plasmid sequentially treated with EcoRI, T4 DNA polymerase, and NotI. The Hy_pMT Laccase2-*circbabo(5,6,7,8S)−3XFlag-stop* and Hy_pMT Laccase2-*3XFlag-stop-circbabo(5,6,7,8S)* constructs were generated by Gibson assembly based on the Hy_pMT Laccase2-*circbabo(5,6,7,8S)* construct. Expression vector for Flag-circbabo(5,6,7,8S)-p: a DNA fragment encoding Flag-tagged circbabo(5,6,7,8S)-p was amplified by PCR and cloned into pUASTattB using EcoRI and XhoI restriction sites, to generate pUASTattB-3-Flag- circbabo(5,6,7,8S)-p. To generate constructs expressing C-terminal HA or Flag-tagged put, full-length put was subcloned into pUASTattB-HA and pUASTattB-flag vectors using XbaI and XhoI restriction sites, respectively. To generate pUASTattB-babo-HA, babo cDNA from clone (RE55648) was amplified and inserted into the pUASTattB-HA vector using EcoRI and XhoI restriction sites. To generate pUASTattB-Smad-HA, Smad cDNA

from clone (LD15813) was amplified and inserted into the pUASTattB-HA vector using XbaI and XhoI restriction sites. To generate pUASTattB-SREBP-HA, SREBP cDNA from clone (LP12374) was amplified and inserted into the pUASTattB-HA vector using XbaI and XhoI restriction sites.

Drosophila genetics

The fly stocks information and the genotypes of the flies used in this study are listed in Additional file 15: Table S4. Flies were maintained at room temperature with standard fly food. The composition of the fly food are as follows: "The fly food media recipe includes the following components, sucrose (40 g/L), dry yeast (25 g/L), cornmeal (66.8 g/L), soy flour (9.1 g/L), agar (6 g/L), maltose (42.4 g/L), sodium benzoate (1 g/L), propionic acid (6.8 mL/L), and Nipagin 15% (2.5 mL/L).

Lifespan assays

We crossed the indicated genotypes of flies with a pan neuronal-specific *nSyb-Gal4* driver. Groups of 160–200 female flies for each genotypes were collected and 15–20 flies were in each group. All the flies were collected at 1 to 3 days old after eclosion and maintained at 25 °C. We transferred the flies to fresh food and recorded deaths every 2 to 3 days, until all the flies were dead.

Cell culture and transfection

SL2 and S2-TM cells were cultured in Schneider's medium (Sigma, S0146) supplemented with 10% heat-inactivated fetal bovine serum (Hyclone), 100 U/mL of penicillin, and 100 μg/mL streptomycin (Invitrogen-GIBCO, Carlsbad, CA) at 25 °C. To overexpress the Hy_pMT Laccase2_circbabo(5,6,7,8S)-Flag construct, transfection was performed by following the calcium phosphate protocol. After 24 h, cells were treated with 25 μM CuSO4 for 2 days for overexpression. To overexpress pUASTattB-related constructs, the plasmids were transfected into cells together with pAC-Gal4 using lipo8000™ (Beyotime, C0533). Two days after transfection, cells were harvested and used for immunoprecipitation assay or western blotting.

RNA extraction and RT-qPCR

Total RNA was extracted with TRIzol reagent (Invitrogen, 15,596,018). RNA samples were reverse transcribed using Superscript III (Invitrogen, 18,080,044). Real-time RT-PCR analysis was performed with the SYBR Green PCR master mix (BioRad, 1,725,275). Relative mRNA levels were calculated by normalization against the endogenous *Rp49* mRNA (internal control). For each experiment, qPCR reactions were performed in triplicate. Oligonucleotides used in this assay are listed in Additional file 16: Table S5.

RNase R treatment

RNase R treatment was performed as the following [70, 71]. RNA samples were either left untreated or treated with RNase R at 37 °C for 30 min. Subsequently, 2 μg of mouse total RNA was added to the samples and the samples were subjected to reverse transcription using Superscript III (Invitrogen). Levels of various circular and linear RNAs were measured by RT-qPCR using the iQ SYBR-green reagents on a CFX384 Real-Time PCR Detection System (Bio-Rad) and normalized against the mouse *gapdh* transcript. Fold changes in RNA levels were calculated using the ΔΔCt method.

RNA-seq data analysis

The RNA-seq data were analyzed as previously described [37]. Briefly, high-quality reads were aligned to the Drosophila reference genome (dm6) using the STAR alignment algorithm (version 2.6.0c) with default parameters [72]. The read count for each gene was extracted using Subread featureCounts (version 2.0.1) [73] based on the FlyBase r6.40 gene annotation. The Bioconductor package edgeR [74] was carried out to characterize differential expression between cg > shcircbabo(5,6,7,8S)-A flies and cg > shGFP controls. Genes with a fold change greater than 1 and a *p*-value less than 0.05 were considered significant. The RNA-seq data were deposited in the NCBI Gene Expression Omnibus with accession number GSE271420.

LD staining

The wandering 3rd *instar* larval fat bodies and adult fly eyes were dissected in PBS and fixed in 4% paraformaldehyde for 1 h. Subsequently, the tissues were rinsed with PBS and incubated with 200 ng/mL Nile Red (Sigma, 72,485) for 5 min followed by washing with PBS. Stained samples were mounted in 80% glycerol with 5 ng/μL DAPI for microscopy analysis.

TG assay

The wandering 3rd *instar* larval fat bodies were dissected in PBS and then homogenized in 100 μL PBS (containing 0.5% Tween 20). The samples were centrifuged at 14,000 rpm for 3 min. Protein content in 10 μl of supernatant sample was measured using the BCA Protein Assay Kit (Beyotime, P0012). The remaining supernatant was immediately heated at 70 °C for 10 min. The resultant supernatants (20 μL) were incubated with either 20 μL triglyceride reagent (Sigma, F6428) or PBS at 37 °C for 30 min. Subsequently, 30 μL of the resultant mixture was transferred to a 96-well plate and incubated with

100 μL free glycerol reagent (Sigma, T2449) for 5 min at 37 °C. Samples were measured at 540 nm using a GloMax plate reader (Promega Inc.; Madison, Wisconsin, USA). Each measurement was repeated three times. The amount of TG in each sample was defined as the total amount of glycerol in the triglyceride reagent–treated sample by subtracting the amount of free glycerol in the untreated samples. TG levels were normalized to the protein content.

ROS assay

For measurement of ROS levels, fly fat body tissue was dissected from 3rd *instar* larvae in Schneiders medium and incubated with 30 μM Dihydroethidium (Beyotime, S0063) for 5 min in a dark chamber on an orbital shaker. The tissues then were washed, mounted on a glass slide, and examined under a confocal laser scanning microscope.

ATP assay

ATP levels were measured by using the ATP testing assay kit (Beyotime, S0026). Briefly, fat body tissue from 3rd *instar* larvae was dissected and lysed in ATP lysis buffer on ice. The lysates were then centrifuged for 10 min at 12,000 *g*. Subsequently, the supernatants were used to measure ATP with the GloMax plate reader (Promega Inc.; Madison, Wisconsin, USA). Each sample was repeated three times, and three independent assays were performed. The ATP levels were calculated according to the standard curve.

Immunoprecipitation

Cells or tissues were collected and resuspended in lysis buffer (50 mM Tris–HCl, pH 7.5, 100 mM NaCl, 10 mM NaF, 1% NP40, 10% glycerol, 1.5 mM EDTA, 1 mM Na_3VO_4, 1X protease inhibitor). The samples were lysed for 30 min at 4 °C. The lysate was centrifuged at 16,000 *g* for 10 min at 4 °C and the supernatant was transferred into a new tube. About 2 μl of anti-HA (proteintech, 51,064–2-AP) or anti-Flag (AlpVHHs, 016–303-001) antibody and 20 μl protein A + G Agarose beads (Beyotime, p2055) were added to the lysate and incubated overnight at 4 °C with constant rotation. Subsequently, the beads were washed 4 times with ice-cold washing buffer, SDS sample buffer was added to the beads, and immunoblot analysis was performed.

Immunoblot

Total lysates were loaded onto 10% SDS-PAGE and transferred to a PVDF membrane. The membrane was blocked with 5% non-fat milk in TBST buffer (50 mM Tris–Cl, pH 7.4, 150 mM NaCl, 0.1% Tween 20) and incubated with primary antibodies: anti-SREBP (1:100) [43], anti-JNK (1:2000; Santa Cruz Biotechnology, sc-571), anti-Flag (1:2000; AlpVHHs, 016–303-001), anti-HA (1:8000; proteintech, 51,064–2-AP), or anti-Tubulin (1:1000; Beyotime, AT819) in 5% BSA in TBST buffer overnight at 4 °C. The membrane was subsequently washed three times with TBST buffer and incubated with secondary antibodies (1:1000; AlpVHHs, 001–402-005, 025–401-005) for 1 h at room temperature. The membrane was then incubated with ECL reagent and exposed.

RNA immunoprecipitation

To pull down the endogenous *circbabo(5,6,7,8S)*, a biotinylated oligo probe complementary to the back-spliced exon junction site of *circbabo(5,6,7,8S)* was applied as previously described [37]. A probe with sense sequence to the back-spliced exon junction serves as a negative control. Briefly, ~ 1×10^8 cells were lysed in 500 μl lysis buffer (20 mM Tris–HCl (pH 7.6), 150 mM NaCl, 2 mM EDTA, 10% glycerol, 1% Triton X-100, 1 mM DTT, 1 mM orthovanadate). Then samples were centrifuged for 10 min at 15,000 rpm, and the supernatant was incubated with 5 μg oligo probe and 30 μl of Streptavidin C1 magnetic beads (Invitrogen, 65,001) were added to the supernatant and incubated for 5 h at room temperature. Next, the beads were washed 3 times with lysis buffer and resuspended with 300 μl 0.4 M NaCl and 300 μl phenol/chloroform/isoamyl alcohol for RNA extraction. The resultant RNA was analyzed by RT-qPCR.

To perform RNA immunoprecipitation using protein as bait, ~ 1×10^8 SL2 cells stably expressing RpL22-TAP or TAP tag only were collected and lysed in 500 μl lysis buffer (20 mM Tris–HCl (pH 7.6), 150 mM NaCl, 2 mM EDTA, 10% glycerol, 1% Triton X-100, 1 mM DTT, 1 mM orthovanadate, 1 X protease inhibitor). About 20 μl IgG Sepharose (GE healthcare, GE17-0969–01) was added into lysates and incubated at 4 °C overnight. The beads were washed 3 times in lysis buffer and resuspended in 0.4 M NaCl. Subsequently, RNA extraction and RT-qPCR were performed to measure levels of various RNAs immune-purified TAP complexes and compared to input samples.

Transmission electron microscopy

Fly heads were dissected and fixed at 4 °C in 2% paraformaldehyde (15,710, Electron Microscopy Sciences) with 2% glutaraldehyde (16,020, Electron Microscopy Sciences) and 0.1 M sodium cacodylate (pH 7.2) (12,201, Electron Microscopy Sciences). Subsequently, the tissues were post-fixed in 2% OsO4 (19,152, Electron Microscopy Sciences). After rinsing three times with PBS, samples were dehydrated via a graded ethanol series (50%, 70%, 80%, 90%, 95%, and 100%, respectively). Subsequently, the samples were dehydrated in propylene

oxide (PO) (82,320, Sigma) for 30 min. Following infiltration with a series of Eponate 12 resin (50% and 75% in PO) and then embedded in a mixture of fresh Eponate 12 resin, made up with Embed 812 (14,900, Electron Microscopy Sciences), DDSA (13,710, Electron Microscopy Sciences), NMA (19,000, Electron Microscopy Sciences), and DMP-30 (13,600, Electron Microscopy Sciences) and polymerized at 65 °C for 48 h. The 50-nm thin sections were cut on Leica EM UC7 ultramicrotome (Leica Microsystems, Vienna, Austria) and stained with 4% uranyl acetate (22,400, Electron Microscopy Sciences) and 2.5% lead nitrate (17,800, Electron Microscopy Sciences) for electron microscopy analysis (HT7700, Hitachi Ltd., Tokyo, Japan).

Immunofluorescence assays

The 3rd *instar* larvae were dissected in PBS and fixed with 4% paraformaldehyde for 1 h at room temperature (RT). The tissues were washed with PBST (0.1% Triton X-100) at RT and incubated with anti-Flag antibodies (1:500; AlpVHHs, 016–303-001) overnight at 4 °C, followed by extensive washing. The tissues were then incubated with Alexa Fluor™ 594 secondary antibodies (1:1000; Invitrogen, A-21203) for 3 h at RT. The samples were mounted in 80% glycerol with 5 ng/μL DAPI. Confocal images were collected using a LSM710 confocal microscope (LSM710, Carl Zeiss, Oberkochen, Germany).

Statistical analysis

All statistical analyses in this manuscript were performed using biological replicates and the sample number (n) is shown for each dataset in the corresponding legend. All analyses were performed in Prism (GraphPad Prism 10). One-way ANOVA with Turkey post hoc test for multiple comparisons and two-tailed unpaired Student's *t* test were performed. Defining lipid droplet size was performed as the following: "Images were imported into the ImageJ software and converted to 8-bit grayscale format with the option of "Type". Next, upon choosing the option of "Adjust", a pop-up window is opened by choosing the option of "Threshold". Next, we set the image as dark background and used the brightness sliding bar to highlight the lipid droplets staining. Subsequently, we quantified the lipid droplets by choosing the "Analyze" menu, then analyzed particles. A new "Result" window then appeared which includes the raw data. Lastly, raw data were exported into Excel. The column of particle areas was used for subsequent statistical analysis. For lifespan assays, the curves represent the average percent survival and a Gehan-Breslow-Wilcoxon test was performed to determine significance. Unless noted otherwise, data is shown in this manuscript as mean values + SEM. A p-value < 0.05 was considered statistically significant.

Abbreviations

circRNAs	Circular RNAs
TG	Triacylglycerols
CE	Cholesterol esters
LDs	Lipid droplets
SREBP	Sterol regulatory element binding protein
ATPCL	ATP citrate lyase
ACACA	Acetyl-CoA carboxylase
FASN	Fatty acid synthase
PI3K	Phosphoinositide 3-kinase
mTOR	Mechanistic target of rapamycin
ROS	Reactive oxygen species
JNK	C-Jun N-terminal kinase
ncRNAs	Non-coding RNAs
lncRNA	Long non-coding RNA
PTBP1	Polypyrimidine tract-binding protein 1
TGF-β	Transforming growth factor-β
shRNA	Small hairpin RNA
UAS	Upstream activating sequence
GFP	Green fluorescent protein
Lsd-1	Lipid storage droplet-1
Lsd-2	Lipid storage droplet-2
Hsl	Hormone-sensitive lipase
Bmm	Brummer

Supplementary Information

The online version contains supplementary material available at https://doi.org/10.1186/s12915-025-02175-1.

Additional file 1: Table S1. circbabo(5,6,7,8S) sequence confirmed by Sanger sequencing. Sanger sequencing uncovered that circbabo(5,6,7,8S) is 1,339-nt in length. The potential open reading frame (ORF) is the green highlighted sequence and two putative start coding sequences are highlighted in purple.

Additional file 2: Fig. S1. circbabo(5,6,7,8S) depletion leads to lipid accumulation. (A-B) A second shRNA transgene (shcircbabo(5,6,7,8S)-C) or the control shGFP was expressed in the fat body under the control of cg-gal4. Nile red and DAPI, respectively, label neutral lipids and nuclei. Scale bar, 50 μm. (C) Quantification of LD size in (A and B) (student t-test, $n = 3$, *** $p<0.001$). (D) TG levels of a similar set of samples as in A and B (fat bodies) were measured and normalized (student t-test, $n = 3$, * $p<0.05$). (E) Total RNA was prepared from the fat bodies of third-instar larvae carrying the indicated transgenes driven by cg-Gal4, and levels of circbabo(5,6,7,8S) were measured (student t-test, $n = 3$, ** $p<0.01$). (F-G) The UAS-shcircbabo(5,6,7,8S)-A or the control UAS-shGFP transgenic flies were crossed to ppl>Gal4 driver flies. Nile red and DAPI staining, respectively, labels neutral lipids and nuclei. Scale bar, 50 μm. (H) Total RNA was extracted from the fat body samples of the indicated genotypes, and levels of circbabo(5,6,7,8S) were measured (student t-test, $n = 3$, *** $p<0.001$). (I) Quantification of LD size in (F and G) (student t-test, $n = 3$, *** $p<0.001$). (J) TG levels in fat bodies of genotypes similar to those in F and G were measured and normalized (student t-test, $n = 3$, ** $p<0.01$).

Additional file 3: Fig. S2. Restoring circbabo(5,6,7,8S) expression rescues LD accumulation phenotype in circbabo(5,6,7,8S)-depleted retina. (A-C) Confocal images showing the Nile red stained retinas from 3-day old flies carrying various combinations of the indicated transgenes under the control of GMR-Gal4. Green arrowheads indicate lipid droplets. Scale bar, 5 μm. (D-F) Flies carrying the GMR-Gal4 driver were crossed to UAS-shcircbabo(5,6,7,8S)-A or control UAS-shGFP flies together with the empty vector. The eyes of 3-day old flies with the indicated genotypes were analyzed by TEM. The glial cells that surround the photoreceptors were shaded with light yellow color. Green arrowheads indicate lipid droplets. LDs were localized in neurons (E), LDs were detected in the glia (F). Scale bar, 2 μm. (G) Quantification of the number of LDs in each ommatidium from flies with the indicated genotypes. (H-J) Confocal images showing the Nile red stained retinas from 3-day old flies carrying various combinations of the indicated transgenes under the control of repo-Gal4. Scale bar, 10 μm. (K) Quantification of the number of intact photoreceptors

in each ommatidium from flies with the indicated genotypes of H-J. Different number of (K=19, H=28, I=24, J=39) ommatidia were counted. (L-Q) Flies carrying the neuronal-specific elav-Gal4 driver were crossed to UAS-shcircbabo(5,6,7,8S)-A or control UAS-shGFP flies together with the empty vector or the UAS-circbabo(5,6,7,8S) transgene. The eyes of 3-day (L-N) or 30-day old (O-Q) flies with the indicated genotypes were analyze. Ommatidia were not affected at day 3 when circbabo(5,6,7,8S) was knocked down but showed moderate degeneration at day 30. The defects were rescued by introducing the UAS-circbabo(5,6,7,8S) transgene. The green arrowheads indicate the lipid droplet structure that was detected in the 3-day old elav>shcircbabo(5,6,7,8S)-A flies. Scale bar, 10 μm. (R and S) Quantification of the number of intact photoreceptors in each ommatidium from flies with the indicated genotypes of L-Q. Different number of (L=14, M=12, N=14, O=13, P=13, Q=14) ommatidia were counted. (T) Quantification of the number of LDs in each ommatidium from flies with the indicated genotypes (one-way ANOVA with Turkey post-hoc test, $n = 3$, *** $p<0.001$).

Additional file 4: Table S2. RNA-seq analysis identifies genes that are impacted by circbabo(5,6,7,8S) depletion in vivo. Total RNA was extracted from Cg>shGFP and Cg>shcircbabo(5,6,7,8S) animals and subjected to RNA-seq. Three biological replicates were analyzed for each sample.

Additional file 5: Fig. S3. Knockdown of SREBP rescues the neurodegeneration and shortened lifespan phenotypes in circbabo(5,6,7,8S)-depleted flies. (A) Total RNA from the fat bodies of indicated genotypes were extracted and RT-qPCR was performed to quantify levels of select RNAs (student t-test, $n = 3$, ** $p<0.01$; *** $p<0.001$; ns, non-significant). (B-I) Various combinations of the indicated transgenes were expressed under the control of cg-Gal4. Nile red and DAPI were employed to label lipid droplets and nuclei, respectively. Overexpression of Bmm, knockdown of Lsd-2, or introducing one copy of SREBP mutant allele rescued the LD accumulation phenotype in cg>shcircbabo(5,6,7,8S) flies. Scale bar, 20 μm. (J) Quantification of LD size in B-I (one-way ANOVA with Turkey post-hoc test, $n = 3$, * $p<0.05$; ** $p<0.01$; *** $p<0.001$). (K-Q) Flies carrying GMR-Gal4 driver were crossed to UAS-shcircbabo(5,6,7,8S)-A or control UAS-shGFP flies together with the empty vector or the one copy of SREBP mutant allele. The eyes of 3-day (K-M) or 30-day old (O-Q) flies with the indicated genotypes were analyze. The retinal defects of shcircbabo(5,6,7,8S) flies were partially rescued by introducing one copy of SREBP mutant allele. Scale bar, 10 μm. (N and R) Quantification of the number of intact photoreceptors in each ommatidium from flies with the indicated genotypes. (S-U) TEM images showing the ultrastructure of retinas from flies with the indicated combinations of transgenes driven by GMR-Gal4. The morphology and number of GMR>shcircbabo(5,6,7,8S) rhabdomeres were severely affected at day 30. Knockdown of SREBP rescues the photoreceptor cell loss phenotype in the GMR>shcircbabo(5,6,7,8S) retina. Scale bar, 5 μm. (V) Quantification of the number of intact photoreceptors in each ommatidium from flies with the indicated genotypes. (W) Lifespan of flies carrying the indicated combinations of transgenes driven by the pan neuronal nSyb-Gal4 driver is shown (n represents number of groups for each genotype, 16-20 flies in each group. shGFP, vector=10; shcircbabo(5,6,7,8S)-A, vector=10; shcircbabo(5,6,7,8S), shSREBP=8).

Additional file 6: Fig. S4. circbabo(5,6,7,8S) is enriched in the RpL22 ribosomal protein complex. (A) Lysates from cells expressing TAP-tagged RpL22, or TAP tag only (negative control) were subjected to immunoprecipitation with IgG agarose beads. Total RNA was extracted from the immune-purified complexes and a fraction of the input samples. Levels of select transcripts were measured by RT-qPCR. Percentage pulldown relative to the input sample is shown. Protein-coding mRNAs Reaper and Rp49 serve as positive controls (student t-test, $n = 3$, ** $p<0.01$; *** $p<0.001$). (B) Schematic of the Flag-stop-circbabo(5,6,7,8S) minigene driven by the metallothionein promoter. The ORF and the corresponding UTR are shown in green and blue, respectively. Positions of the initiation codon and stop codon are noted. A 3X FLAG epitope tag-coding sequence was placed immediately upstream of the putative stop codon. (C) S2-TM cells were transfected with empty vector, the circbabo(5,6,7,8S) minigene or the Flag-stop-circbabo(5,6,7,8S) minigene described in B. Cell lysates from two independent pools of stably transfected S2-TM cells carrying the Flag-stop-circbabo(5,6,7,8S) minigene were subject to anti-Flag immunoprecipitation, and immunopurified complexes were subjected to immunblot using anti-Flag antibody.

Additional file 7: Table S3. Mass spectrometry analysis identifies proteins from the immuno-purified anti-Flag samples. Lysate from SL2 cells stably expressing circbabo(5,6,7,8S)-Flag was subjected to immunoprecipitation using the anti-Flag antibody, Then the purfied samples were subjected to mass spectrometry.

Additional file 8: Fig. S5. circbabo(5,6,7,8S)-p does not directly interact with SREBP but modulates TGF-β signaling, as revealed by RNA-seq and KEGG analysis. (A) circbabo(5,6,7,8S)-p and SREBP did not interact with each other. Various combinations of expression constructs for Flag-tagged circbabo(5,6,7,8S)-p and HA-tagged SREBP were transfected into S2 cells. Both 10% of cell lysates and immuno-purified HA and Flag complexes were analyzed by immunoblot. (B) Immunostaining of Flag-circbabo(5,6,7,8S)-p with the Flag antibody showed cytoplasmic distribution in fat body cells. Scale bar, 50 μm. (C) KEGG pathway enrichment analysis of RNA-seq data ($p<0.05$). Count: number of target genes in each pathway; Gene ratio: the ratio of the number of target genes divided by the number of all the genes in each pathway. TGF-β signaling pathway was highlighted with a red line box.

Additional file 9: Fig. S6. Knockdown of SREBP rescues the LD accumulation phenotype elicited by babo.Q302D overexpression. (A-D) Various combinations of the indicated transgenes were expressed in the fat body under the control of cg-Gal4. Knockdown of SREBP rescues the LD accumulation phenotype elicited by babo.Q302D overexpression. Scale bar, 20 μm. (E) Quantification of LD size in A, B, C, and D (one-way ANOVA with Turkey post-hoc test, $n = 4$, ** $p<0.01$; *** $p<0.001$). (F-G) Overexpression of babo.Q302D under the control of GMR-Gal4 led to LD accumulation in retinas. Green arrowheads indicate lipid droplets. White arrowhead indicates abnormal retina. Scale bar, 5 μm.

Additional file 10: Fig. S7. babo interacts with put. Flag tagged put could pull-down HA tagged babo in S2 cells. Various combinations of expression constructs for Flag-tagged put and HA-tagged babo were transfected into S2 cells. Both 10% of cell lysates and immuno-purified HA and Flag complexes were analyzed by immunoblot.

Additional file 11: Fig. S8. babo.Q302D overexpression or circbabo(5,6,7,8S) depletion leads to mitochondrial dysfunction. (A) The indicated transgenes were expressed in the fat body under the control of cg-Gal4. ATP levels in fat-body tissues were measured (one-way ANOVA with Turkey post-hoc test, $n = 3$, * $p<0.01$; *** $p<0.001$). (B, C, E, F, and G) The indicated transgenes were expressed in the fat body under the control of cg-Gal4. ROS levels in the fat-body of indicated genotypes were measured by DCF staining and analyzed by confocal microscopy. Scale bar, 50 μm. (D and H) Quantification of the DCF fluorescence intensity in the indicated genotypes (and one-way ANOVA with Turkey post-hoc test, $n = 4$-5, * $p<0.05$; ** $p<0.01$; *** $p<0.001$).

Additional file 12: Fig. S9. Overexpression of hSOD1 rescues LD accumulation and photoreceptor cell loss phenotypes in circbabo(5,6,7,8S)-depleted flies. (A-F) Flies carrying the eye-specific GMR-Gal4 driver were crossed to UAS-shcircbabo(5,6,7,8S)-A or control UAS-shGFP flies together with the empty vector or the UAS-hSOD1 transgene. The eyes of 3-day old flies with the indicated genotypes were analyzed. Overexpression of hSOD1 rescued the LD accumulation and photoreceptor cell loss phenotypes in GMR>shcircbabo(5,6,7,8S) flies. The green arrowheads indicate the lipid droplet structure that was detected in the 3-day old GMR>shcircbabo(5,6,7,8S)-A flies. Scale bars for A-C, 2 μm; for D-F, 10 μm. (G) Quantification of the number of LDs in each ommatidium from flies with the indicated genotypes. (one-way ANOVA with Turkey post-hoc test, $n = 3$, *** $p<0.001$). (H) Quantification of the number of intact photoreceptors in each ommatidium from flies with the indicated genotypes of D-F. Different number of (D=13, E=14, F=20) ommatidia were counted.

Additional file 13: Fig. S10. The LD accumulation phenotype elicited by circbabo(5,6,7,8S) depletion is not dependent on Relish or FoxO. (A-D) Various combinations of the indicated transgenes were expressed in the fat body under the control of cg-gal4. Nile red and DAPI, respectively, label neutral lipids and nuclei. Knockdown of Relish (Rel) or FoxO did not

impact the LD accumulation phenotype of circbabo(5,6,7,8S)-depleted fat bodies. Scale bar, 50 µm. (E) Quantification of LD size in A, B, C, and D (one-way ANOVA with Turkey post-hoc test, $n = 3$-4, *** $p<0.001$; ns, non-significant).

Additional file 14: Fig. S11. Levels of JNK are elevated upon circbabo(5,6,7,8S) depletion or babo.Q302D overexpression in the fat body. (A) The indicated transgenes were expressed in the fat body under the control of cg-gal4. Immunoblot shows circbabo(5,6,7,8S) depletion or babo.Q302D overexpression in the fat body leads to an increase in total JNK levels compared to the shGFP (control). (B) shows the quantification of results in A. The experiment has been repeated 3 times (one-way ANOVA with Turkey post-hoc test, $^{**}p < 0.01$; $^{***}p < 0.001$).

Additional file 15: Table S4. Genotypes of flies analyzed and fruit fly reagents used in this study.

Additional file 16: Table S5. Oligos used in this study.

Acknowledgements
We are grateful to THFC, BDSC, CEMCS, and DGRC for providing fly strains and cDNA clones. We thank Dr. Chao Tong and Dr. Jun-Zheng Zhang for the fly stocks. We thank Dr. Jeremy Wilusz for the Hy_pMT Laccase2 MCS exon vector; Dr. Jun-Yuan Ji for antibody against SREBP; Dr. Akhila Rajan for protocol for lipid assays; Dr. Robert Cole for advice on mass spectrometry analysis; Dr. Wei-Na Shang for advice on transmission electron microscopy analysis. We thank Drs. Timothy Osborne and Ranjan Perera for insightful suggestions. JS is supported by Scientific Research Foundation for Excellent Talents of Xuzhou Medical University [D2022048]. WL is supported by National Natural Science Foundation of China [32200622], Scientific Research Foundation for Excellent Talents of Xuzhou Medical University [D2022049, TD202404]. RZ is supported by the National Institutes of Health [1R01AI140049, 1R21AI131099] and Johns Hopkins University. JLL is supported by the Intramural Research Program of the National Institute of Environmental Health Sciences [ZIC ES103371].

Authors' contributions
Conceptualization: JS, XMZ, WHL, JFL, BZ, JM, AX, JWL, JLL, RZ, WL; Methodology: JS, XMZ, WHL, JFL, BZ, JM, AX, XXY, JWL, JLL, RZ, WL; Investigation: JS, XMZ, WHL, JFL, BZ, JM, AX, XXY, JWL, JLL, RZ, WL; Visualization: JS, WL, RZ; Supervision: WL, RZ; Writing—original draft: JS, WL, RZ; Writing—review & editing: JS, WHL, WL, JLL, RZ; All authors read and approved the final manuscript.

Funding
JS is supported by Scientific Research Foundation for Excellent Talents of Xuzhou Medical University [D2022048]. WL is supported by National Natural Science Foundation of China [32200622], Scientific Research Foundation for Excellent Talents of Xuzhou Medical University [D2022049, TD202404]. RZ is supported by the National Institutes of Health [1R01AI140049, 1R21AI131099] and Johns Hopkins University. JLL is supported by the Intramural Research Program of the National Institute of Environmental Health Sciences [ZIC ES103371].

Data availability
All data generated or analysed during this study are included in this published article, its supplementary information files and publicly available repositories. All data and the original blots have been included in figshare (https://doi.org/10.6084/m9.figshare.28365836.v1) [75]. RNA-seq dataset is available from Gene Expression Omnibus (GSE271420). The mass-spectrometry data can be found on figshare (https://doi.org/10.6084/m9.figshare.28365836.v1) [75].

Declarations

Ethics approval and consent to participate
Not applicable.

Consent for publication
Not applicable.

Competing interests
The authors declare no competing interests.

Author details
[1]Jiangsu Key Laboratory of Brain Disease and Bioinformation, Research Center for Biochemistry and Molecular Biology, Xuzhou Medical University, Xuzhou 221004, China. [2]Departments of Medicine, Biological Chemistry & Oncology, Johns Hopkins University School of Medicine, Johns Hopkins All Children'S Hospital, BaltimoreSt. Petersburg, MDFL 2120533701, USA. [3]Department of Medicine, Brown University, Providence, RI 02912, USA. [4]National Institute of Environmental Health Sciences, Durham, NC 27709, USA.

Received: 22 July 2024 Accepted: 21 February 2025
Published online: 05 March 2025

References

1. Yoon H, Shaw JL, Haigis MC, Greka A. Lipid metabolism in sickness and in health: Emerging regulators of lipotoxicity. Mol Cell. 2021;81(18):3708–30.
2. Zadoorian A, Du X, Yang H. Lipid droplet biogenesis and functions in health and disease. Nat Rev Endocrinol. 2023;19(8):443–59.
3. Olzmann JA, Carvalho P. Dynamics and functions of lipid droplets. Nat Rev Mol Cell Biol. 2018;20(3):137–55.
4. Mathiowetz AJ, Olzmann JA. Lipid droplets and cellular lipid flux. Nat Cell Biol. 2024;26(3):331–45.
5. Bosch M, Sánchez-Álvarez M, Fajardo A, Kapetanovic R, Steiner B, Dutra F, et al. Mammalian lipid droplets are innate immune hubs integrating cell metabolism and host defense. Science. 2020;370(6514):eaay8085.
6. Ralhan I, Chang CL, Lippincott-Schwartz J, Ioannou MS. Lipid droplets in the nervous system. J Cell Biol. 2021;220(7):21.
7. Alassaf M, Rajan A. Diet-induced glial insulin resistance impairs the clearance of neuronal debris in Drosophila brain. PLoS Biol. 2023;21(11): e3002359.
8. Wang G, Yin W, Shin H, Tian Q, Lu W, Hou SX. Neuronal accumulation of peroxidated lipids promotes demyelination and neurodegeneration through the activation of the microglial NLRP3 inflammasome. Nat Aging. 2021;1(11):1024–37.
9. Yang LG, March ZM, Stephenson RA, Narayan PS. Apolipoprotein E in lipid metabolism and neurodegenerative disease. Trends Endocrinol Metab. 2023;34(8):430–45.
10. Marschallinger J, Iram T, Zardeneta M, Lee SE, Lehallier B, Haney MS, et al. Lipid-droplet-accumulating microglia represent a dysfunctional and pro-inflammatory state in the aging brain. Nat Neurosci. 2020;23(2):194–208.
11. Haney MS, Pálovics R, Munson CN, Long C, Johansson PK, Yip O, et al. APOE4/4 is linked to damaging lipid droplets in Alzheimer's disease microglia. Nature. 2024;628(8006):154–61.
12. Grabner GF, Xie H, Schweiger M, Zechner R. Lipolysis: cellular mechanisms for lipid mobilization from fat stores. Nat Metab. 2021;3(11):1445–65.
13. Yang L, Liang J, Lam SM, Yavuz A, Shui G, Ding M, et al. Neuronal lipolysis participates in PUFA-mediated neural function and neurodegeneration. EMBO Rep. 2020;21(11): e50214.
14. Girard V, Jollivet F, Knittelfelder O, Celle M, Arsac J-N, Chatelain G, et al. Abnormal accumulation of lipid droplets in neurons induces the conversion of alpha-Synuclein to proteolytic resistant forms in a Drosophila model of Parkinson's disease. PLoS Genet. 2021;17(11): e1009921.
15. Haidar M, Loix M, Bogie JFJ, Hendriks JJA. Lipophagy: a new player in CNS disorders. Trends Endocrinol Metab. 2021;32(11):941–51.
16. Duan X, Xu L, Li Y, Jia L, Liu W, Shao W, et al. Regulation of lipid homeostasis by the TBC protein dTBC1D22 via modulation of the small GTPase Rab40 to facilitate lipophagy. Cell Rep. 2021;36(9):109541.
17. Lan Z-q, Ge Z-y, Lv S-k, Zhao B, Li C-x. The regulatory role of lipophagy in central nervous system diseases. Cell Death Discov. 2023;9(1):229.
18. Li Y, Munoz-Mayorga D, Nie Y, Kang N, Tao Y, Lagerwall J, et al. Microglial lipid droplet accumulation in tauopathy brain is regulated by neuronal AMPK. Cell Metab. 2024;36(6):1351–70.e8.
19. Jung WH, Liu CC, Yu YL, Chang YC, Lien WY, Chao HC, et al. Lipophagy prevents activity-dependent neurodegeneration due to dihydroceramide accumulation in vivo. EMBO Rep. 2017;18(7):1150–65.
20. Jeon YG, Kim YY, Lee G, Kim JB. Physiological and pathological roles of lipogenesis. Nat Metab. 2023;5(5):735–59.
21. Shimano H, Sato R. SREBP-regulated lipid metabolism: convergent physiology — divergent pathophysiology. Nat Rev Endocrinol. 2017;13(12):710–30.

22. Chandel NS. Lipid Metabolism. Cold Spring Harb Perspect Biol. 2021;13(9): a040576.
23. Piccolis M, Bond LM, Kampmann M, Pulimeno P, Chitraju C, Jayson CBK, et al. Probing the Global Cellular Responses to Lipotoxicity Caused by Saturated Fatty Acids. Mol Cell. 2019;74(1):32–44.
24. Li X, Zhang M, Liu M, Liu TH, Hemba-Waduge RU, Ji JY. Cdk8 attenuates lipogenesis by inhibiting SREBP-dependent transcription in Drosophila. Dis Model Mech. 2022;15(11):14.
25. Yecies JL, Zhang HH, Menon S, Liu S, Yecies D, Lipovsky AI, et al. Akt stimulates hepatic SREBP1c and lipogenesis through parallel mTORC1-dependent and independent pathways. Cell Metab. 2011;14(1):21–32.
26. Laplante M, Sabatini DM. mTORC1 activates SREBP-1c and uncouples lipogenesis from gluconeogenesis. Proc Natl Acad Sci U S A. 2010;107(8):3281–2.
27. Liu L, Zhang K, Sandoval H, Yamamoto S, Jaiswal M, Sanz E, et al. Glial Lipid Droplets and ROS Induced by Mitochondrial Defects Promote Neurodegeneration. Cell. 2015;160(1):177–90.
28. Olive V, Minella AC, He L. Outside the coding genome, mammalian microRNAs confer structural and functional complexity. Sci Signal. 2015;8(368):re2.
29. Xiao M-S, Ai Y, Wilusz JE. Biogenesis and Functions of Circular RNAs Come into Focus. Trends Cell Biol. 2020;30(3):226–40.
30. Lyu J, Chen Y, Yang W, Guo T, Xu X, Xi Y, et al. The conserved microRNA miR-210 regulates lipid metabolism and photoreceptor maintenance in the Drosophila retina. Cell Death Differ. 2021;28(2):764–79.
31. Liu C, Yang Z, Wu J, Zhang L, Lee S, Shin DJ, et al. Long noncoding RNA H19 interacts with polypyrimidine tract-binding protein 1 to reprogram hepatic lipid homeostasis. Hepatology. 2018;67(5):1768–83.
32. Xiong X-P, Liang W, Liu W, Xu S, Li J-L, Tito A, et al. The circular RNA Edis regulates neurodevelopment and innate immunity. PLoS Genet. 2022;18(10): e1010429.
33. Liu W, Liang W, Xiong X-P, Li J-L, Zhou R. A circular RNA Edis-Relish-castor axis regulates neuronal development in Drosophila. PLoS Genet. 2022;18(10): e1010433.
34. Pamudurti NR, Patop IL, Krishnamoorthy A, Bartok O, Maya R, Lerner N, et al. circMbl functions in cis and in trans to regulate gene expression and physiology in a tissue-specific fashion. Cell Rep. 2022;39(4): 110740.
35. Arcinas C, Tan W, Fang W, Desai TP, Teh DCS, Degirmenci U, et al. Adipose circular RNAs exhibit dynamic regulation in obesity and functional role in adipogenesis. Nat Metab. 2019;1(7):688–703.
36. Liu CX, Chen LL. Circular RNAs: Characterization, cellular roles, and applications. Cell. 2022;185(12):2016–34.
37. Liang W, Liu W, Xiong X-P, Li JW, Li J-L, Perera RJ, et al. The circular RNA circATP8B(2) regulates ROS production and antiviral immunity in Drosophila. Cell Rep. 2024;43(4): 113973.
38. Li Q, Yao H, Wang Y, Wu Y, Thorne RF, Zhu Y, et al. circPRKAA1 activates a Ku80/Ku70/SREBP-1 axis driving de novo fatty acid synthesis in cancer cells. Cell Rep. 2022;41(8):111707.
39. Song W, Owusu-Ansah E, Hu Y, Cheng D, Ni X, Zirin J, et al. Activin signaling mediates muscle-to-adipose communication in a mitochondria dysfunction-associated obesity model. Proc Natl Acad Sci U S A. 2017;114(32):8596–601.
40. Estes RE, Lin B, Khera A, Davis MY. Lipid Metabolism Influence on Neurodegenerative Disease Progression: Is the Vehicle as Important as the Cargo? Front Mol Neurosci. 2021;14:788695.
41. Davie K, Janssens J, Koldere D, De Waegeneer M, Pech U, Kreft Ł, et al. A Single-Cell Transcriptome Atlas of the Aging Drosophila Brain. Cell. 2018;174(4):982–98.e20.
42. Martínez BA, Hoyle RG, Yeudall S, Granade ME, Harris TE, Castle JD, et al. Innate immune signaling in Drosophila shifts anabolic lipid metabolism from triglyceride storage to phospholipid synthesis to support immune function. PLoS Genet. 2020;16(11):e1009192.
43. Xie X-J, Hsu F-N, Gao X, Xu W, Ni J-Q, Xing Y, et al. CDK8-Cyclin C Mediates Nutritional Regulation of Developmental Transitions through the Ecdysone Receptor in Drosophila. PLoS Biol. 2015;13(7): e1002207.
44. Beller M, Bulankina AV, Hsiao H-H, Urlaub H, Jäckle H, Kühnlein RP. PERILIPIN-Dependent Control of Lipid Droplet Structure and Fat Storage in Drosophila. Cell Metab. 2010;12(5):521–32.
45. Pamudurti NR, Bartok O, Jens M, Ashwal-Fluss R, Stottmeister C, Ruhe L, et al. Translation of CircRNAs. Mol Cell. 2017;66(1):9–21.
46. Wesselhoeft RA, Kowalski PS, Anderson DG. Engineering circular RNA for potent and stable translation in eukaryotic cells. Nat Commun. 2018;9(1):2629.
47. Gu Y, Mao Y, Jia L, Dong L, Qian S-B. Bi-directional ribosome scanning controls the stringency of start codon selection. Nat Commun. 2021;12(1):6604.
48. Zheng X, Wang J, Haerry TE, Wu AY, Martin J, O'Connor MB, et al. TGF-beta signaling activates steroid hormone receptor expression during neuronal remodeling in the Drosophila brain. Cell. 2003;112(3):303–15.
49. Upadhyay A, Moss-Taylor L, Kim MJ, Ghosh AC, O'Connor MB. TGF-β Family Signaling in Drosophila. Cold Spring Harb Perspect Biol. 2017;9(9):a022152.
50. Zhu CC, Boone JQ, Jensen PA, Hanna S, Podemski L, Locke J, et al. Drosophila Activin-β and the Activin-like product Dawdle function redundantly to regulate proliferation in the larval brain. Development. 2008;135(3):513–21.
51. Zaiatz-Bittencourt V, Finlay DK, Gardiner CM. Canonical TGF-β Signaling Pathway Represses Human NK Cell Metabolism. J Immunol. 2018;200(12):3934–41.
52. Sun X, Lu Q, Yegambaram M, Kumar S, Qu N, Srivastava A, et al. TGF-β1 attenuates mitochondrial bioenergetics in pulmonary arterial endothelial cells via the disruption of carnitine homeostasis. Redox Biol. 2020;36(101593):31.
53. Sanchez JA, Mesquita D, Ingaramo MC, Ariel F, Milán M, Dekanty A. Eiger/TNFα-mediated Dilp8 and ROS production coordinate intra-organ growth in Drosophila. PLoS Genet. 2019;15(8): e1008133.
54. Seo E, Kang H, Choi H, Choi W, Jun H-S. Reactive oxygen species-induced changes in glucose and lipid metabolism contribute to the accumulation of cholesterol in the liver during aging. Aging Cell. 2019;18(2): e12895.
55. Blas-García A, Apostolova N, Ballesteros D, Monleón D, Morales JM, Rocha M, et al. Inhibition of mitochondrial function by efavirenz increases lipid content in hepatic cells. Hepatology. 2010;52(1):115–25.
56. Yan H, Ding M, Peng T, Zhang P, Tian R, Zheng L. Regular Exercise Modulates the dfoxo/dsrebp Pathway to Alleviate High-Fat-Diet-Induced Obesity and Cardiac Dysfunction in Drosophila. Int J Mol Sci. 2023;24(21):15562.
57. Fowler JWM, Zhang R, Tao B, Boutagy NE, Sessa WC. Inflammatory stress signaling via NF-kB alters accessible cholesterol to upregulate SREBP2 transcriptional activity in endothelial cells. eLife. 2022;11:e79529.
58. Ito M, Nagasawa M, Omae N, Tsunoda M, Ishiyama J, Ide T, et al. A novel JNK2/SREBP-1c pathway involved in insulin-induced fatty acid synthesis in human adipocytes. J Lipid Res. 2013;54(6):1531–40.
59. Legnini I, Di Timoteo G, Rossi F, Morlando M, Briganti F, Sthandier O, et al. Circ-ZNF609 Is a Circular RNA that Can Be Translated and Functions in Myogenesis. Mol Cell. 2017;66(1):22–37.e9.
60. Zhang M, Zhao K, Xu X, Yang Y, Yan S, Wei P, et al. A peptide encoded by circular form of LINC-PINT suppresses oncogenic transcriptional elongation in glioblastoma. Nat Commun. 2018;9(1):018–06862.
61. Chen C-K, Cheng R, Demeter J, Chen J, Weingarten-Gabbay S, Jiang L, et al. Structured elements drive extensive circular RNA translation. Mol Cell. 2021;81(20):4300–18.e13.
62. Shaw WM, Luo S, Landis J, Ashraf J, Murphy CT. The C. elegans TGF-β Dauer Pathway Regulates Longevity via Insulin Signaling. Curr Biol. 2007;17(19):1635–45.
63. Bai H, Kang P, Hernandez AM, Tatar M. Activin Signaling Targeted by Insulin/dFOXO Regulates Aging and Muscle Proteostasis in Drosophila. PLoS Genet. 2013;9(11): e1003941.
64. Haynes PR, Pyfrom ES, Li Y, Stein C, Cuddapah VA, Jacobs JA, et al. A neuron–glia lipid metabolic cycle couples daily sleep to mitochondrial homeostasis. Nat Neurosci. 2024;27(4):666–78.
65. Liu L, MacKenzie KR, Putluri N, Maletić-Savatić M, Bellen HJ. The Glia-Neuron Lactate Shuttle and Elevated ROS Promote Lipid Synthesis in Neurons and Lipid Droplet Accumulation in Glia via APOE/D. Cell Metab. 2017;26(5):719–37.e6.
66. Ioannou MS, Jackson J, Sheu S-H, Chang C-L, Weigel AV, Liu H, et al. Neuron-Astrocyte Metabolic Coupling Protects against Activity-Induced Fatty Acid Toxicity. Cell. 2019;177(6):1522–35.e14.
67. Lee H, Cho S, Kim M-J, Park YJ, Cho E, Jo YS, et al. ApoE4-dependent lysosomal cholesterol accumulation impairs mitochondrial homeostasis and oxidative phosphorylation in human astrocytes. Cell Rep. 2023;42(10):113183.

68. Yang D, Wang X, Zhang L, Fang Y, Zheng Q, Liu X, et al. Lipid metabolism and storage in neuroglia: role in brain development and neurodegenerative diseases. Cell Biosci. 2022;12(1):106.
69. Kramer MC, Liang D, Tatomer DC, Gold B, March ZM, Cherry S, et al. Combinatorial control of Drosophila circular RNA expression by intronic repeats, hnRNPs, and SR proteins. Genes Dev. 2015;29(20):2168–82.
70. Xiong X, Liang W, Liu W, Xu S, Li J, Tito A, et al. The Circular RNA Edis Regulates Neurodevelopment and Innate Immunity. PLoS Genet. 2022;18(10):e1010429.
71. Rybak-Wolf A, Stottmeister C, Glazar P, Jens M, Pino N, Giusti S, et al. Circular RNAs in the Mammalian Brain Are Highly Abundant, Conserved, and Dynamically Expressed. Mol Cell. 2015;58(5):870–85.
72. Dobin A, Davis CA, Schlesinger F, Drenkow J, Zaleski C, Jha S, et al. STAR: ultrafast universal RNA-seq aligner. Bioinformatics. 2013;29(1):15–21.
73. Liao Y, Smyth GK, Shi W. featureCounts: an efficient general purpose program for assigning sequence reads to genomic features. Bioinformatics. 2014;30(7):923–30.
74. McCarthy DJ, Chen Y, Smyth GK. Differential expression analysis of multifactor RNA-Seq experiments with respect to biological variation. Nucleic Acids Res. 2012;40(10):4288–97.
75. Sheng J, Zhang X-M, Liang W-H, Lyu J-F, Zhang B, Min J, et al. The circular RNA circbabo(5,6,7,8S) regulates lipid metabolism and neuronal integrity via TGF-β/ROS/JNK/SREBP signaling axis in Drosophila. figshare. Dataset. 2025. https://doi.org/10.6084/m9.figshare.28365836.v1.

Publisher's Note